1984ApJ...280..825B

THE ASTROPHYSICAL JOURNAL, 280:825–847, 1984 May 15
© 1984. The American Astronomical Society. All rights reserved. Printed in U.S.A.

THE EVOLUTION AND FATE OF VERY MASSIVE OBJECTS

J. R. BOND
Institute for Theoretical Physics, Department of Physics, Stanford University; and
Institute, of Astronomy, Cambridge University
W. D. ARNETT
Astronomy and Astrophysics Center, University of Chicago
AND
B. J. CARR
Institute of Astronomy, Cambridge University
Received 1982 July 26; accepted 1983 August 23

ABSTRACT

The structure and evolution of Very Massive Objects (stars of mass $\sim 10^2$–$10^5\ M_\odot$) are discussed in terms of simple semianalytic models. We estimate the helium enrichment due to mass loss, and present evidence for a dynamical instability arising in the hydrogen shell burning phase of a 500 $M_\odot$ Population I star. The fate of a VMO is decided in its oxygen core phase, Calculations of the effects of the pair instability, oxygen and silicon burning, and alpha-quenching on the global binding energy of initially isentropic polytropic cores allow us to predict the critical oxygen core mass above which complete collapse to a black hole occurs: $M_{\rm Oc} \approx 10^2\ M_\odot$ corresponding to an initial star mass greater than 200 $M_\odot$. Cores smaller than this explode; we estimate the kinetic energy liberated.

Subject headings: stars: interiors — stars: massive

I. INTRODUCTION

We define Very Massive Objects (VMOs) to be those stars which are pair unstable during their oxygen core phase. For stars of Population III, which we take here to mean those of nearly zero metallicity, the mass range of VMOs extends from $\sim 10^2$ to $\sim 10^5\ M_\odot$. Because of the paucity of VMOs in the present epoch, the theory of their stellar evolution has not been well developed. VMOs are, however, excellent candidates for Population III stars. The lack of metals and the influence of the cosmic background radiation at early times may shift the fragmentation mass spectrum of star-forming clouds to larger scales than those inferred to arise from Population I and II clouds (Hartquist and Cameron 1977; Silk 1977; Tohline 1980; Silk 1980; Kashlinsky and Rees 1983). In a companion paper (Carr, Bond, and Arnett 1984, hereafter CBA), we study the cosmological consequences of Population III stars, with special emphasis on the potential role of VMOs in solving various cosmological riddles. In particular, they could produce: black holes (the dark matter problem); an early injection of heavy elements with accompanying abundance anomalies (the G dwarf problem, and the oxygen anomaly at low metallicity); a nonprimordial source of helium; spectral distortions in the microwave background (Woody and Richards 1979); significant contributions to other radiation bands; explosive injection of supernova energy into the pregalactic and protogalactic medium with its potential role in galaxy formation (Ostriker and Cowie 1981; Ikeuchi 1981). To quantify these possibilities, we need a detailed understanding of the stellar evolution and fate of Population III VMOs, which we provide in this paper by utilizing a variety of analytical and numerical methods. Some results of this work have been previously reported (Bond, Arnett, and Carr 1982; Carr, Arnett, and Bond 1982; Arnett, Bond, and Carr 1982; Bond, Carr, and Arnett 1983).

The possibility that a physical mechanism exists which limits the upper range of stellar masses has received much attention over the years. The standard stellar evolution texts of the 1960s pointed to the nuclear pulsational instability in radiation-dominated stars (Ledoux 1941) as the reason there are few, if any, very massive stars (e.g., Cox and Giuli 1968). In the early 1970s, a number of workers showed that if hydrodynamical nonlinearities are taken into account, the pulsational amplitude remains finite, and the mass loss rate, though perhaps quite large, is also finite.

Larson and Starrfield (1971) suggested that an upper mass limit for stars arises as a result of processes which occur during formation. Collapse of a $\gamma < 4/3$ gas is nonhomologous which leads to a strong central condensation, an embryo star upon which matter from the protostellar envelope is accreted. They estimated the time scale for accretion by assuming the envelope of a given mass protostar begins collapsing at the free-fall rate when its density has risen to the point at which it is just marginally Jeans unstable. As a result, the cooler the cloud, the longer the accretion time for a region of the same mass due to the smaller density required for the Jeans instability. The temperature of molecular clouds from which stars form now (~ 20 K) is determined by grain cooling. In this case, they estimate that the accretion time exceeds the time for the star to contract to the main sequence and ignite hydrogen if $M \gtrsim 6\ M_\odot$. Certainly this cannot represent an upper mass limit. However, they show that radiation pressure on grains, radiative heating, and H II region formation prior to complete envelope

© American Astronomical Society • Provided by the NASA Astrophysics Data System

1984ApJ...280..825B

accretion all conspire to limit the star mass to values less than about 60–100 $M_\odot$. These analytic arguments are supported by the numerical calculations of spherically symmetric massive star formation by Appenzeller and Tscharnuter (1974) and Yorke and Krügel (1977). Though these processes may explain why there are so few very massive stars around, they do not exclude their formation for a variety of reasons: (1) Regions more massive than the Jeans mass would collapse faster than the marginally Jeans unstable region. (2) Deviations from spherical geometry due to rotatonal flattening, clumpy infall, and coalescence of protostellar regions would considerably modify these limits. (3) If stellar collapse is pressure-driven—for example, by externally applied shock waves from supernovae or by expanding H II bubbles—one can clearly get higher mass collapses. (4) In dense star clusters, such as may occur in active galactic nuclei, star collisions may lead to very massive star formation (Begelman and Rees 1978). Indeed, the standard models for quasars and active galactic nuclei require that large black holes form, presumably from either a VMO or a Supermassive Object (SMO) ($M > 10^5\ M_\odot$). The required precursor star depends upon the efficiency of accretion for the lower mass holes, but would likely be at least $10^3\ M_\odot$ (Duncan and Shapiro 1983).

In a Population III cloud, there are no grains to keep the temperature low. Accretion from a 10^4 K neutral hydrogen gas which is marginally Jeans unstable occurs much more quickly ($\sim 2M/M_\odot$ yr^{-1}) than from a 20 K gas for a protostar of the same mass. Consequently, Larson and Starrfield's value of 6 $M_\odot$ goes up to $\sim 5 \times 10^4\ M_\odot$, which we obtained by computing the Kelvin-Helmholtz time for Population III VMOs, $t_{\rm KH} \sim 3 \times 10^4\ (M/10^3\ M_\odot)^{1/23}$ yr. The effects of molecular hydrogen cooling in dense regions can lower the temperature below 10^4 K, to ~ 300 K, corresponding to a limit of $\sim 300\ M_\odot$. In any case, the upper mass boundary is higher without grains, making the formation of some VMOs more likely.

It has often been suggested that there may even be a *lower* mass boundary in the VMO range for metal-free stars (Yoneyama 1972; Hutchins 1976; Tohline 1980). These arguments usually involve the details of molecular hydrogen cooling. Recently, Palla, Salpeter, and Stahler (1983) have shown that at high densities, molecular cooling is enhanced by three-body effects, with the result that solar-type stars could form in Population III environments. However, if the first stars formed at a redshift above 100, when the background radiation had a temperature in excess of 300 K, the formation of molecular hydrogen would be inhibited, though it could still have appeared at high density. Though the minimum possible stellar mass is certainly larger in metal-free regions than in those with grains, we can only take this as suggesting that VMOs could be much more numerous at early epochs.

In this paper, we step through the various stages in the evolution of VMOs, illustrating how simple agruments, often based on the distribution, generation, and transmutation of entropy, can be used to understand quantitatively many of the steps. In particular, in § II, we analyze the hydrogen and helium burning phase of VMO evolution using the Eddington standard model and the point source model with special emphasis upon Population III abundances. We present simple calculations of the helium loss due to winds, and of the various boundaries that define VMOs. In § III, the evolution of the oxygen core is analyzed by considering the transmutations of the entropy that occur as a consequence of the pair instability, nuclear burning, and alpha-quenching. We calculate the changes in the core's binding energy during these three processes to determine the fate of the core. More detailed descriptions of the content of the many subsections of §§ II and III are given at the beginning of the respective sections. In § IV, we present our conclusions regarding the state of VMO research.

II. VMO EVOLUTION THROUGH CORE HYDROGEN AND HELIUM BURNING

In this section, we discuss the main features of early VMO evolution. In § II*a* we review the pulsational mass loss estimates. In § II*b* we utilize entropy in discussing the Eddington standard model and the predictions of luminosity, central temperature and density, stellar radius, and surface temperature. We then provide a simple explanation of the characteristic CNO abundance $\sim 10^{-9}$ found in Population III models, which is so fundamental to their structure. In § II*c*, we use the point source model to refine the estimates made in § II*b*. Formulae for the evolution of the convective core fraction and for the helium core mass are derived. The lifetime of VMOs is then calculated. In § II*d*, evolution with mass loss is discussed, and the yield of helium from winds is derived. In § II*e*, we present a model of a 500 $M_\odot$ star in which the hydrogen envelope is ejected by a super-Eddington luminosity generated in a hydrogen burning shell. In § II*f*, we consider the Eddington model of the helium core, and use it to calculate the helium ignition temperature. In § II*g*, the mass boundary between VMOs and SMOs is calculated using general relativistic polytropes.

a) Mass Loss in VMOs

The calculation of the mass loss rate driven by the nuclear pulsational instability poses a difficult problem in nonlinear hydrodynamics, and only incomplete theoretical information is now available.

Upon ignition of hydrogen, VMOs become unstable, energized by the fusion reactions in their stellar cores (Ledoux 1941), provided their mass is in excess of the critical pulsational mass for hydrogen burning:

$$M_p \approx (108 + 20X_\alpha)(1 - 5X_\alpha/8)^2\ M_\odot\ . \qquad (1)$$

This formula is a fit to the Population II calculations of Stothers and Simon (1970). Here, X_α is the fraction of baryons in helium. If primordial helium has a mass fraction $X_\alpha = 0.25$, then M_p is predicted to be 80 $M_\odot$. Higher metallicities give higher pulsational masses; e.g., for a solar Population I composition, $M_p = 91\ M_\odot$. Ziebarth (1970) presents a fitting formula for his Population I results which gives $M_p = 88\ M_\odot$ for solar composition, in good agreement with Stothers and Simon. These values are higher than the often quoted 60 $M_\odot$ limit of Schwarzschild and Härm (1959), which incorporated only the electron scattering opacity. Boury (1963) has estimated $M_p \sim 260\ M_\odot$ for pure hydrogen stars.

Linear instability analysis predicts that the amplitude of the fundamental radial oscillation mode which is fed by the nuclear energy input grows exponentially, with *e*-folding times of the order of 1000 years, since the envelope cannot successfully radiate the excess energy. As the hydrogen is

© American Astronomical Society • Provided by the NASA Astrophysics Data System

1984ApJ...280..825B

consumed, the abundance gradient would act to increase the e-folding time. However, if $M \gg M_p$, there are so many e-folding times that the surface velocities would quickly exceed the escape velocity, with mass loss so large that M would fall below M_p on time scales small compared with the hydrogen burning time, as Schwarzschild and Härm detailed in their classic 1959 paper. Since stars apparently exist with masses in excess of their M_p, they suggested that the inclusion of nonlinear terms would aid in damping the fundamental mode, resulting in a finite amplitude of oscillation.

The nonlinear hydrodynamical equations describing the limiting of the pulsational amplitude in zero-age main sequence VMOs were solved by a number of workers in the early 1970s (Appenzeller 1970; Talbot 1971; Zeibarth 1970; Papaloizou 1973), each with varying degrees of approximation, since the e-folding times for linear growth were so much greater than the pulsational periods ($\sim\frac{1}{2}$ day). They all found that the mode steepens to create shocks in the envelope, which propagate to the surface, driving mass loss at a large but finite rate. The amplitude does indeed self-limit itself. Talbot (1971) found the fractional variation in the radius in the center of the star reaches a maximum value of about one-tenth. As an abundance gradient forms, this amplitude presumably goes down, finally reaching stability before complete hydrogen exhaustion. The actual mass loss rate associated with these radial pulsations is difficult to calculate, since it requires very detailed zoning in the outer layers to see radial zones lifted to beyond the escape velocity. None of the estimates given can be regarded as reliable.

b) *The Eddington Standard Model for VMOs*

The dimensionless entropy per baryon in photons and in gas, pure numbers, provides useful characterizations of the thermodynamic structure of VMOs. In convective cores, mixing is rapid relative to evolutionary time scales, and the abundance distribution is homogeneous. A homogeneous core is convectively unstable if the specific entropy decreases outward. Convection then acts to make the core isentropic, and the value of the entropy per baryon characterizes the temperature-density relation. For VMOs on the main sequence, electrons are nondegenerate (n.d.) and nonrelativistic (n.r.), so their entropy is given by the usual Sackur-Tetrode expression,

$$s_e = Y_e(\tfrac{5}{2} - \mu_e/T)\,, \tag{2}$$

where Y_e is the number of electrons per baryon, the inverse of the electron molecular weight often used, μ_e is the electron chemical potential (with the rest mass subtracted out), and T is the temperature in energy units (Boltzmann constant = 1). The entropy of each species of nucleus, j, is similarly

$$s_j = Y_j\left(\frac{5}{2} - \frac{\mu_j}{T}\right) = Y_j\left\{\frac{5}{2} - \ln\frac{n_B\, Y_j}{g_j}\frac{[2\pi(\hbar c)^2]^{3/2}}{[A_j m_N\, T]^{3/2}}\right\}, \tag{3}$$

where Y_j is the number per baryon, n_B is the baryon density, m_N is the nucleon mass, and g_j is the statistical weight of nucleus j (the partition function at high temperature). The nuclear entropy, s_N, is then the sum of all the s_j's. For example, if we have pure hydrogen and helium,

$$s_N = Y_I\left[18.80 + \ln\left(\frac{T^{3/2}}{\rho}\right)\right] - Y_p \ln\left(\frac{Y_p}{2}\right) - Y_\alpha \ln\left(\frac{Y_\alpha}{8}\right), \tag{4}$$

where T is measured in keV, ρ is measured in g cm^{-3}, and $Y_I = Y_p + Y_\alpha$ is the inverse of the usual ionic weight μ_I. A similar expression holds for s_e. The number of nuclei plus electrons per baryon is $Y_T \equiv Y_I + Y_e$, the inverse of the total molecular weight. Notice that $Y_T = 2(1 - 5X_\alpha/8)$, which is the reason this curious combination entered equation (1) for M_p. The electron plus ion pressure is just $p_g = T_T n_B T$. The photon entropy,

$$s_\gamma = \frac{4}{3}\frac{\pi^2}{15(\hbar c)^3}\frac{T^3}{n_B} = 0.19\frac{T^3}{\rho}\,, \tag{5}$$

is a very useful parameter for stellar interior work, since it is related to β, the ratio of gas pressure to total pressure, by

$$\sigma \equiv s_\gamma/(4Y_T) = (\beta^{-1} - 1)\,. \tag{6}$$

For a pure H-He star with $Y_p = 0.78$, $X_\alpha = 0.22$ (where generally $X_j \equiv A_j Y_j$ gives the fraction of baryons in species j), we have $Y_e = 0.89$ and $Y_T = 1.73$, so radiation pressure accounts for half of the total when $s_\gamma = 4Y_T \sim 7$. The total entropy is

$$s = s_e + s_N + s_\gamma \equiv s_g + s_\gamma\,. \tag{7}$$

In the center of the Sun, the gas entropy, s_g, is now ~ 19; the photon entropy is only ~ 0.003. In VMOs, s_g depends only weakly upon the stellar mass; it is ~ 35. The photon entropy rises with the mass, ranging from 5 to 100 as we now show.

For radiation-dominated stars, convective equilibrium will yield $s_\gamma \approx$ constant. This is the equation of state (EOS) for a $n = 3$ polytrope, provided the abundances are spatially homogeneous, suggesting such models may do quite well for zero-age main sequence VMOs. The polytropic mass is related to s_γ by

$$M_3(s_\gamma) = 0.6(m_P{}^3/m_N{}^2)s_\gamma{}^2(p/p_\gamma)^{3/2} \tag{8a}$$

$$= 1.1 s_\gamma{}^2(1 + 4Y_T/s_\gamma)^{3/2}\, M_\odot \text{ (n.d., n.r. electrons)}, \tag{8b}$$

which holds provided the right-hand side is constant throughout the star. Here, m_P is the Planck mass, 1.22×10^{22} MeV. This is Eddington's famous quartic equation expressed in slightly different language from that usually seen. We denote by $\bar{s}_\gamma$ the solution of $M = M_3(s_\gamma)$; $\bar{\sigma}$ can be read off Figure 1. Radiation dominance is predicted to occur for $M > M_3(7) \approx 155\, M_\odot$.

VMOs radiate at a considerable fraction of the Eddington limit appropriate for Thomson scattering, L_{ED}. Our Eddington model prediction is

$$L/L_{ED} = (4Y_T/s_\gamma + 1)^{-1}\,, \tag{9a}$$

$$L_{ED} = M(3m_N{}^2/2m_P{}^3)(m_e/\alpha^2 m_N)(m_e/m_P{}^{-1})Y_e{}^{-1}$$

$$= 1.2 \times 10^{38}\, Y_e{}^{-1}\, M/M_\odot \text{ ergs s}^{-1}\,. \tag{9b}$$

The adiabatic indices

$$\Gamma_1 \equiv \left(\frac{\partial \ln p}{\partial \ln n_B}\right)_s = \frac{4}{3} + \frac{1}{3}(1 + 4\sigma)(1 + \sigma)^{-1}(1 + 8\sigma)^{-1}\,, \tag{10}$$

$$\Gamma_4 \equiv 1 + \frac{p}{n_B \epsilon} = \frac{4}{3} + \frac{1}{3}(2\sigma + 1)^{-1}\,,$$

determine whether the star is dynamically unstable (the pressure average of Γ_1 being less than 4/3) or unbound

© American Astronomical Society • Provided by the NASA Astrophysics Data System

1984ApJ...280..825B

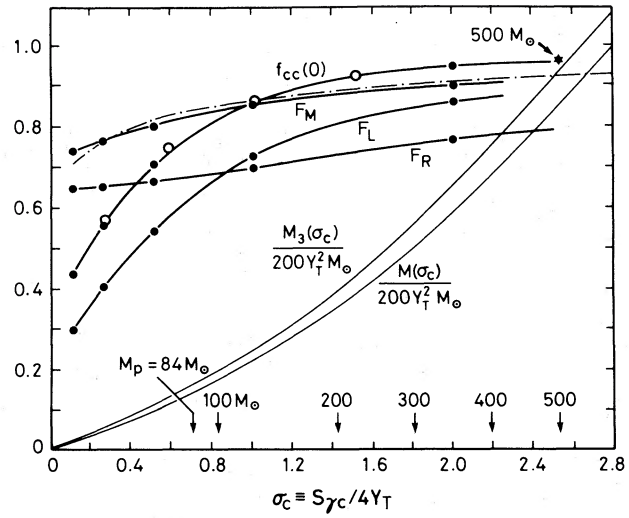

FIG. 1.—Point source model modification factors for the mass, luminosity, and radius are given as a function of the central photon entropy paramenter, σ_c, or equivalently of the star mass. The initial convective core mass fraction, $f_{cc}(0)$, for zero-age main sequence VMO models is also shown. The closed circles are Henrich's (1943) points, and the open circles are those of Schwarzschild and Härm (1958); the 500 $M_\odot$ point is for the star of Fig. 2. The M_3 curve can be used to get $\bar{\sigma}$, and the M curve to get σ_c.

(the pressure average of Γ_4 being less than 4/3). Here, ϵ is the internal energy per baryon. For the 80 $M_\odot$ polytrope, $\Gamma_1 = 1.46$ and $\Gamma_4 = 1.49$. Even for a 1000 $M_\odot$ polytrope, $s_\gamma = 25$, $\Gamma_1 = 1.37$, and $\Gamma_4 = 1.37$. These numbers are sufficiently far from $\Gamma = 4/3$ that a more realistic model is required: the point source model of § IIc.

The central temperature can be expressed in terms of the entropy and the metallicity by equating the nuclear energy generated to the luminosity—which is known from equations (8) and (9). We derive this expression in Appendix A, following the method of Fowler and Hoyle (1964). Accurate approximations over the VMO range are:

$$T_c = 3.8\left(\frac{\sigma^2}{1+\sigma}\right)^{0.054}\left(\frac{X_{CN}}{0.01}\right)^{-0.054} \text{ keV},$$

Population I and II; (11a)

$$T_c = 11.3\left(\frac{\sigma^2}{1+\sigma}\right)^{0.087}\left(\frac{X_{CN}}{10^{-9}}\right)^{-0.079} \text{ keV},$$

Population III. (11b)

The weakness of the mass dependences, $\sim M^{0.03}$ and $\sim M^{0.04}$, respectively, shows that all VMOs have nearly the same central temperature. The metallicity dependence is also weak. However, the very large difference between CNO abundances of stars with Population I or II abundances and those of Population III—which initially have no CNO nuclei, and must generate them through the 3α reaction—translates into a significantly higher central temperature required for Population III stars to support the given luminosity. Here, σ should be evaluated at the center, and is generally not equal to $\bar{\sigma}$.

The radius is sensitive to the outer structure of the star: in the $n = 3$ polytrope approximation,

$$R_3(\sigma) = 6.9[p_c/(\pi G\rho_c^2)]^{1/2} = 30.4\, Y_T \sigma^{1/2}(1+\sigma)^{1/2} T_c(\sigma)^{-1} R_\odot , \quad (12)$$

where T_c is in keV. The radii so predicted are ~20%–30% too high. Given $L_3(\sigma)$ from equation (9), we can determine the surface temperature:

$$T_{e3}(\sigma) = 2.44 T_c(\sigma)^{1/2} Y_e^{-1/4}(1+\sigma^{-1})^{-1/8} \text{ eV} . \quad (13)$$

Similar formulae have been given by Fowler and Hoyle (1964) for massive stars and by Wagoner (1969) for SMOs. Notice that the surface temperature is almost mass-independent: $T_e \sim 10^5$ K $\sigma^{0.04}$ for Population III, and $\sim 6 \times 10^4$ K $\sigma^{0.03}$ for Population I and II.

The $\sim 10^{-9}$ CNO abundance generated in Population III stars can be simply understood. We sketch the general idea here; the details are given in Appendix B. The star undergoes Kelvin-Helmholtz contraction while very slowly generating CNO nuclei via the triple-alpha reaction. This defines a curve in T_c-X_{CN} space. X_{CN} is monotonically increasing in time, and can be used as a measure of the passage of time. Contraction ceases once the combined energy generation of hydrogen and helium burning can support the star. This thermal equilibrium defines another curve in T_c-X_{CN} space. The CNO abundance at the intersection of these two curves is

$$X_{CN} \approx 2 \times 10^{-10}\sigma^{0.7}(1+\sigma)^{-0.5} \times \left[\left(\frac{X_\alpha}{0.25}\right)^{0.8}\left(\frac{Y_p}{0.75}\right)^{-0.7}\left(\frac{Y_T}{1.7}\right)^{0.2}\left(\frac{Y_e}{0.88}\right)^{-0.5}\right] . \quad (14)$$

The true trajectory followed in T_c-X_{CN} space will pass smoothly from the first curve to the second, settling on the second at a CNO abundance in excess of equation (14). Thus, equation (14) represents a definite lower bound. In Table 1, we show that this bound is not very different from the zero-age main sequence values of El Eid, Fricke, and Ober (1983). As nuclear burning proceeds, the low 3α rate will continually create some CNO nuclei; the star then evolves along the thermal equilibrium line toward increasing X_{CN}. The explicit time dependence is given by equation (B12).

c) *The Point Source Model and the Convective Core*

VMOs in the hydrogen burning phase have large isentropic chemically homogeneous cores upon which are smoothly joined radiative envelopes in which photon transport is dominated by Thomson scattering. These point source models (Cox and Giulli 1968) were first constructed by Henrich (1943) for chemically homogeneous stars. Using his models, the properties of zero-age main-sequence VMOs can be given in terms of the single parameter σ_c. The operational procedure is as follows: (1) Given the initial abundances, determine Y_T. (2) Given M, find σ_c using Figure 1. The relations $M(\sigma_c)$ and $F_M(\sigma_c) = M(\sigma_c)/M_3(\sigma_c)$ can be determined analytically as we demonstrate in Appendix C. The approximation

$$\sigma_c(M) \approx 0.24 Y_T^{-1}(M/M_\odot)^{1/2} - 0.61, \quad M > 10^2 M_\odot , \quad (15)$$

is accurate over the VMO range. (3) Use σ_c in equation (11) to obtain T_c, and equation (5) to obtain ρ_c. (4) The radius is then found from $R = F_R(\sigma_c)R_3(\sigma_c)$, the luminosity from

© American Astronomical Society • Provided by the NASA Astrophysics Data System

1984ApJ...280..825B

TABLE 1

HYDROGEN BURNING PHASE PREDICTIONS

M; Pop	$X_{\alpha i}$; $X_{\rm CNO}$	σ_c	T_c	ρ_c	$s_{\gamma c}$	s_{gc}	$L/L_{\rm ED}$	$R/R_\odot$	T_e	$\bar{\sigma}$	$f_{cc}(0)$	M_z/M_i	$\tau_{\rm H}$
T10[2]	0.27	0.90	3.82	1.79	5.89	34.8	0.32	12.1	4.72	...	...	...	...
I	0.01	0.88	3.83	1.86	5.73	34.7	0.32	12.6	4.63	0.79	0.84	0.49	3.0
T10[3]	0.27	4.06	4.40	0.61	26.5	36.9	0.74	42.9	5.46	...	...	...	...
I	0.01	4.03	4.26	0.56	26.3	36.9	0.78	43.3	5.51	3.90	0.98	0.57	2.0
T10[4]	0.27	14.2	4.81	0.23	92.7	38.7	0.91	142	5.62	...	...	...	...
I	0.1	14.0	4.60	0.20	91.4	38.8	0.92	148	5.52	13.9	0.998	0.57	1.7
KS10[3]	0.0	3.33	15.0	24	26.6	41.2	0.81	14.7	9.22	...	0.92	0.5	2.8
III	8(−11)	3.17	15.4	27	25.3	41.0	0.76	14.1	9.25	3.1	0.98	0.49	3.3
EFO80	0.26	0.72	10.4	44.7	4.82	32.8	0.31	3.79	7.84	...	0.80	0.35	3.4
III	8(−10)	0.74	10.6	45.2	4.95	32.8	0.27	3.72	7.67	0.62	0.79	0.46	3.5
EFO100	0.26	0.86	11.1	45.0	5.78	32.9	0.36	4.10	8.29	...	0.84	0.40	3.1
III	5(−10)	0.86	11.1	44.8	5.76	32.9	0.31	4.01	8.09	0.76	0.84	0.48	3.3
EFO150	0.26	1.15	11.3	35.7	7.70	33.3	0.46	5.21	8.66	...	0.89	0.46	2.7
III	7(−10)	1.16	11.2	34.6	7.77	33.4	0.41	5.09	8.53	1.06	0.89	0.51	2.9
EFO200	0.26	1.42	11.2	28.2	9.51	33.7	0.53	6.32	8.74	...	0.91	0.49	2.4
III	1.1(−9)	1.43	11.1	27.3	9.57	33.7	0.48	6.23	8.59	1.32	0.92	0.53	2.7
EFO300	0.26	1.87	11.4	22.5	12.5	34.1	0.62	8.04	8.92	...	0.94	0.52	2.2
III	1.4(−9)	1.90	11.3	21.5	12.7	34.2	0.56	8.09	8.68	1.76	0.95	0.54	2.5
EFO500	0.26	2.56	11.9	18.7	17.1	34.6	0.72	10.5	9.24	...	0.97	0.55	2.0
III	1.3(−9)	2.58	11.8	17.8	17.3	34.6	0.65	10.5	9.02	2.46	0.97	0.56	2.3
2000	0.25	–	...	...									
I	0.01	5.82	4.15	0.35	38.6	38.2	0.85	76.5	5.05	5.68	0.99	0.57	2.0

NOTE.—M is in $M_\odot$, T_c in keV, ρ_c in g cm^{-3}, T_e in eV, and $\tau_{\rm H}$ in 10^6 yr. Our predictions are on the second line of each entry. The initials of the numerical models refer to: T = Talbot (1971); KS = Kovetz and Shaviv (1971); EFO = El Eid, Fricke, and Ober (1983). The CNO abundances on the second line come from the models. M_z/M_i is calculated from eq. (21) which is applicable only if the mass loss never exceeds the critical rate. In the EFO runs, the mass loss rate sometimes exceeds critical, hence the discrepancies. $f_{cc}(0)$ and $\tau_{\rm H}$ are calculated using $\bar{\sigma}$.

$L = F_L(\sigma_c)L_3(\sigma_c)$, and the surface temperature from the $T_e \sim L^{1/4}R^{-1/2}$ relation. Here, the correction factors which we infer from the Heinrich results, F_L and F_R, are plotted in Figure 1. The expression

$$F_R(\sigma) = \min\{1, 0.64 + 0.06\sigma\}$$

is a good approximation for the latter. In Table 1, we compare the values we predict for stars of various masses and compositions with the numerical models of Talbot (1971), Kovetz and Shaviv (1971), and the recent work of El Eid, Fricke, and Ober (1983). The agreement is excellent.

The magnitude of the deviation of the point source model from the $n = 3$ polytrope can be made explicit by considering the variation in the photon entropy. Within the convective core, $s_g + s_\gamma$ is constant; hence

$$\rho/\rho_c = (s_\gamma/s_{\gamma c}) \exp[8\sigma(s_\gamma/s_{\gamma c} - 1)] . \quad (16a)$$

An approximate solution to this transcendental equation, which is accurate for large σ as long as $\rho/\rho_c > \exp(-8\sigma)$, is

$$s_\gamma/s_{\gamma c} = (\rho/\rho_c)^{1/(1+8\sigma)} . \quad (16b)$$

For $s_{\gamma c} = 10$, $s_\gamma(r)$ falls to 9.4, 8.2, and 6.4 for $\rho/\rho_c = 0.5$, 0.1, and 0.01, respectively.

The luminosity is given exactly by a modified version of equation (9) (provided electron scattering dominates the opacity):

$$L = 1.2 \times 10^{38} Y_{\rm es}^{-1}(1 + \sigma_s^{-1})^{-1} M/M_\odot \text{ ergs s}^{-1} , \quad (17)$$

where σ_s and $Y_{\rm es}$ are surface values. Unfortunately, we have found no analytic way to estimate σ_s, and hence $F_L(\sigma_c)$.

The major trends in the evolution of the mass fraction of the convective core at time t, $f_{cc}(t)$, can be understood by exploiting the constancy of the luminosity over the radiative envelope. In particular, at the boundary between the convective core and the radiative envelope, the entropy gradient vanishes ($\nabla s = 0$); if we neglect abundance gradients, the radiative luminosity can then be written as

$$L = 1.2 \times 10^{38}\left(\frac{M_{cc}}{M_\odot}\right) Y_{\rm ecc}^{-1}(1 + \sigma_{cc}^{-1})^{-1} \times \left[1 - \frac{3}{8(1 + \sigma_{cc})(1 + 4\sigma_{cc})}\right]^{-1} \text{ergs s}^{-1} , \quad (18)$$

where σ_{cc} and $Y_{\rm ecc}$ are evaluated at the edge of the convective core. Here, M_{cc} is the convective core mass.

© American Astronomical Society • Provided by the NASA Astrophysics Data System

1984ApJ...280..825B

Equating this expression with equation (17) yields

$$f_{cc}(t) = \frac{M_{cc}(t)}{M} = \left(\frac{Y_{ecc}}{Y_{es}}\right) \frac{\sigma_s}{1+\sigma_s} \frac{(5/8 + 5\sigma_{cc} + 4\sigma_{cc}^2)}{\sigma_{cc}(1+4\sigma_{cc})} \quad (19a)$$

$$\rightarrow Y_{ecc}/Y_{es} \quad \text{as} \quad \sigma_s, \sigma_{cc} \rightarrow \infty \, . \quad (19b)$$

Consider first the zero-age main sequence behavior: $Y_{ecc} = Y_{es}$. We clearly get the trend of the convective core mass fraction increasing with mass toward its asymptote of unity. We can do no better without a detailed numerical model to get σ_s and σ_{cc}. Henrich's values of $f_{cc}(0)$ are plotted in Figure 1; for $\bar{\sigma}$ in the VMO range, it is fitted by the formula

$$f_{cc}(0) \approx 1 - [3(\bar{\sigma})^{1/2}(1+\bar{\sigma})^{3/2}]^{-1} \, .$$

Since $\bar{\sigma} = 0.7$ corresponds to the pulsational boundary mass $M_p = 84\ M_\odot$, the convective core size for these initial models should lie between 0.8 and 1, as all numerical models verify. (See Table 1.) Our 500 $M_\odot$ star with $\sigma = 2.53$ has $f_{cc}(0) = 0.97$, in agreement with the prediction.

For large mass cores, the convective core size obeys equation (19b), which corresponds to $L = L_{ED}$ in each mass zone between the core boundary and the surface. Even though σ_c begins only at 2.53, and σ_{cc} is lower, this simple equation provides a remarkable fit to our 500 $M_\odot$ convective core evolution as we display in Figure 2. The evolved stars of Schwarzschild and Härm (1958) and Kovetz and Shaviv (1971) also follow this law. As hydrogen is depleted, Y_e goes down, and the core size must diminish in step in order to ensure Eddington-limited radiative output throughout the envelope. The final convective core mass fraction for large Population III VMOs is predicted to be 0.5/0.89 = 0.56. When the initial convective core size is not nearly unity, a better estimate of the evolution of M_{cc} in M-Y_e space in the absence of mass loss is:

$$M_{cc}(Y_e)/M = (Y_e/Y_{es}) f_{cc}(0) \, . \quad (20)$$

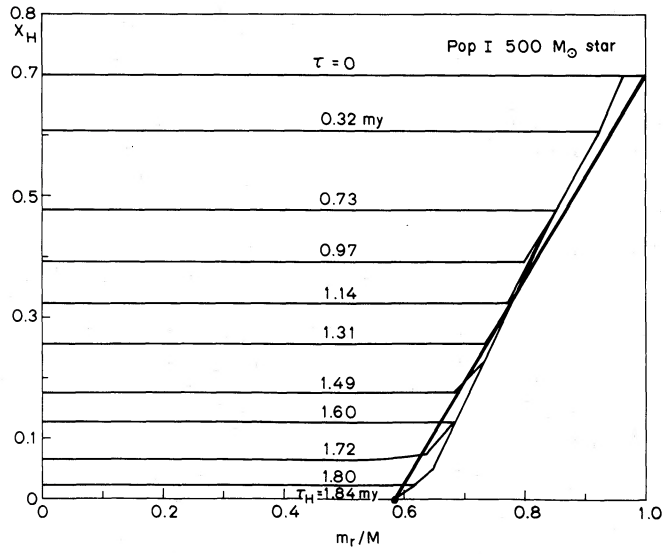

FIG. 2.—The evolution of the hydrogen abundance with time is plotted against mass fraction for our 500 $M_\odot$ Population I star. The core hydrogen burning phase lasted $\tau_H = 1.84 \times 10^6$ yr. The heavy line shows the simple prediction of § IIc for the convective core mass fraction.

This implies an $M_\alpha(M_i)$ relation, where i refers to initial values:

$$M_\alpha/M_i = (2Y_{ei})^{-1} f_{cc}(0) \, . \quad (21)$$

The time it takes the star to exhaust its hydrogen is obtained by integrating the energy balance equation, $0.007 M_{cc}\, c^2 dY_p/dt + L = 0$, between the initial H abundance and its final value of zero. The lifetime computation assumes equation (9) for L and equation (20) for M_{cc}; we obtain

$$\tau_H = 1.7 \times 10^6 (1 + \bar{\sigma}^{-1}) Y_{pi}(1 + Y_{pi}/2) f_{cc}(0) \text{ yr}, \quad (22)$$

where Y_{pi} is the initial hydrogen abundance. Schwarzschild and Härm (1958) evolved 121 and 218 $M_\odot$ Population I stars; their nuclear lifetimes, 3.8 and 2.8 million years, respectively, agree with the predictions of equation (22). More comparisons are given in Table 1.

d) Mass Loss and Helium Ejection

Talbot and Arnett (1971) suggested that stellar layers which have processed helium mixed in with their primordial allotment could be lost in a nuclear-pulsation-driven wind, thereby enriching the primordial gas with helium. The mass fraction (relative to the star's initial mass) of newly synthesized helium ejected, $\langle \Delta X_\alpha \rangle$, is related to the mass loss history, $M(t)$, by

$$\langle \Delta X_\alpha \rangle = \int_{M_f}^{M_i} 2[Y_{ei} - Y_{es}(t)] \frac{dM(t)}{M_i} \, , \quad (23)$$

where M_i and M_f are the initial and final star masses. The surface helium abundance can be expressed in terms of the surface electron abundance by $X_{\alpha s}(t) = 2[1 - Y_{es}(t)]$; $Y_{ei} = Y_{es}(0)$ is an initial value. We need only know $Y_{es}(M)$ to compute this integral.

There are two basic types of behavior this function can have, and these can best be understood in Y_e-M space, or equivalently in the Y_p-M space of Figure 2. If the mass loss rate is slower than the nuclear burning rate, the convective core will recede from the stellar surface: $Y_{es}(M)$ will be a straight line beginning at Y_{ei} and following the convective core profile, $Y_e = Y_{ei} M/M_i$, down to the final mass. M_f must necessarily be greater than the $M_{cc}(\tau_H) = 0.5 M_i/Y_{ei}$ computed in § IIc in order for the profile $Y_{es}(M) = Y_{ei} M/M_i$ to be valid. Equation (23) then gives

$$\langle \Delta X_\alpha \rangle = Y_{ei}(1 - M_f/M_i)^2 \, . \quad (24)$$

If the mass loss rate exceeds the nuclear burning rate, the $Y_{es}(M)$-curve again begins at Y_{ei}, but always lies above the convective core curve determined for no mass loss: $Y_{es}(M) > Y_{ei} M/M_i$. More generally, $Y_{es}(M - dM) > Y_{es}(M)(1 - dM/M)$, which translates into the critical instantaneous mass loss rate

$$(-\dot{M}/M)_{cr} = L/(0.007 Mc^2)(2Y_{es})^{-1}$$

$$= (L/L_{ED}) Y_{es}^{-2} (6.65 \times 10^6 \text{ yr})^{-1} \, , \quad (25a)$$

$$(-\dot{M})_{cr} = 1.5 \times 10^{-5} (M/100\ M_\odot)(L/L_{ED}) Y_{es}^{-2}\ M_\odot \text{ yr}^{-1} \, . \quad (25b)$$

The associated time scale is near the nuclear burning time. As long as $-\dot{M}$ remains under $-\dot{M}_{cr}$, equation (20) for the convective core evolution and equation (21) for the M_α-M_i relation should remain valid. This explains why M_α is insensitive to mass loss provided it is not too large. The

© American Astronomical Society • Provided by the NASA Astrophysics Data System

1984ApJ...280..825B

El Eid, Fricke, and Ober (1983) loss rates are at times in excess of critical; this accounts for the discrepancies between our predictions and their results.

The convective core in the large $\dot{M}$ case maintains a mass fraction near unity throughout the mass loss period for large VMOs. If we also assume that the VMO radiates at nearly the Eddington luminosity, then the surface abundance can be obtained by solving the energy balance equation, $L_{ED} = -0.007Mc^2 2dY_e/dt$. The simple relation

$$Y_{es}(t)^2/Y_{ei}^2 = 1 - (t/\tau_{H0})[1 - (4Y_{ei}^2)^{-1}]$$

follows, where τ_{H0} is the hydrogen burning lifetime given by equation (22) in the limit $s_\gamma \to \infty$. The helium loss is then

$$\langle \Delta X_\alpha \rangle = 2Y_{ei} \int_{M_f}^{M_i} \left(1 - \left\{1 - [1 - (4Y_{ei}^2)^{-1}]\left[\frac{t(M)}{\tau_{H0}}\right]\right\}^{1/2}\right)\frac{dM}{M_i}$$

$$\to \left(\frac{\tau_L}{\tau_{H0}}\right)[1 - (4Y_{ei}^2)^{-1}]Y_{ei} \quad \text{if} \quad \tau_L \ll \tau_{H0} . \qquad (26)$$

To obtain the time at which the mass is M, $t(M)$, a model is needed for $\dot{M}$. The simple limit given in equation (26) holds when the time scale $\tau_L = -M/\dot{M}$ is sufficiently short that one can expand in the small t/τ_{H0}. It is not surprising that very large mass loss rates lead to small helium yields.

The maximum possible yield occurs when the mass loss rate is just that needed for the $Y_e(M)$ profile to follow the $Y_{ei}M/M_i$ curve down to the final convective core mass. Equation (24) can then be used to obtain the maximum

$$\langle \Delta X_\alpha \rangle_{max} = Y_{ei}[1 - (2Y_{ei})^{-1}]^2 , \qquad (27)$$

which is 0.17 if we take $X_{\alpha i} = 0.22$ and hence $Y_{ei} = 0.89$; this is the same as the maximum value estimated by Talbot and Arnett. If $X_{\alpha i} = 0$, $\langle \Delta X_\alpha \rangle_{max} = 0.25$. We now argue that a loss of this magnitude may be realized in large VMOs, not because of the pulsational instability, but because of a dynamical instability which can leave the helium core as remnant while the remaining helium-rich envelope is lifted off.

e) *Hydrogen Shell Burning and Envelope Ejection*

We have evolved a 500 $M_\odot$ Population I star (assuming no mass loss) from initial contraction onto the zero-age main sequence to the onset of core helium burning by using an implicit-hydrodynamical stellar evolution code described in Arnett (1972) and Arnett (1977). Convection is treated as time-dependent and can occur only on time scales associated with the buoyancy forces exerted on eddies. Effects of hydrogen depletion can be seen in Figure 2: the size of the convective core gradually decreases, as described above, until it reaches a final value of $M_\alpha = 0.56\ M_i$. At core hydrogen exhaustion, the luminosity is constant and almost Eddington from the helium core to the surface. As the helium core contracts, hydrogen ignites in a shell surrounding the core. At the shell temperature, $T_s = 4.9$ keV, energy is generated at the rate $\dot{q}_{CN} = 2 \times 10^6$ ergs g^{-1} s^{-1}. At this point, the central temperature is $T_c = 10$ keV, which is approximately given by the simple $n = 3$ polytrope expression T_s/θ, where $\theta \approx 0.5$ is the Lane-Emden function at the shell. Hydrogen shell ignition occurs well before helium ignition in this Population I star: not until $T_c = 20.7$ keV does the helium generation rate reach $\dot{q}_{3\alpha} = 3 \times 10^6$ ergs g^{-1} s^{-1}. (After helium ignition, the core eventually becomes convective out to $M_{cc}/M_i = 0.56$, covering almost the entire helium core; the energy loss is still regulated by radiative diffusion through the small outer layer of the helium core.)

The energy input into the hydrogen shell drives it toward high luminosity. However, the envelope already has the maximum radiative luminosity that can be transported by the outer layers. If we neglect local σ-gradients, this is given by equation (17), except that M, Y_e, and σ (or β) are interior rather than surface values. In the hydrogen burning shell, $1-\beta$ increases from 0.83 to 0.91, and σ from 4.9 to 10.1; to maintain local stability would limit the radiative luminosity to a 10% increase. The actual jump in luminosity is 29%. Consequently, the burning shell becomes convective. The change in radiation entropy (3.8) is much less than the change in gas entropy over the envelope; the outer boundary of the convective zone is limited to $m(r)/M = 0.71$. About 2.5 $M_\odot$ of hydrogen are consumed on a local thermal time scale, releasing 3.5×10^{52} ergs; this compares with a total gravitational binding energy of only 0.5×10^{52} ergs. By the time the envelope expands to recombination conditions, the expansion velocity is supersonic; this "stellar wind" is expected to continue until most of the envelope is stripped off.

This calculation has two flaws: the hydrodynamics was heavily damped, which is a limitation of all implicit codes (Arnett 1977), and the recombination wave was not examined in detail. However, since the energy liberated explosively is so large, 3×10^{52} ergs $\sim 3 \times 10^{-5}\ Mc^2$, we do not expect the latter to be of much importance. It is clear that the low binding energy and large luminosity do make such objects prime candidates for violent mass loss.

The discussion would be different for Population III objects. Since our Population I star has a CNO catalyst abundance ~ 0.01, the hydrogen in the shell ignites *before* the helium core. If we naively scale the CNO rate by the abundance factor of $10^{-9}/10^{-2} = 10^{-7}$, then we would predict that the hydrogen shell ignites *after* the core in Population III VMOs; though in error due to the differing temperature dependences of H and He burning rates, this illustrates that the actual abundance of CNO catalysts in the hydrogen shell may determine qualitative features of the evolution. Woosley and Weaver (1982) evolved a 500 $M_\odot$ Population III star using an implicit-hydrodynamical code similar to the one employed here except that they chose a different scheme to treat time-dependent convection. They find that, though their envelope is driven to very low density, it does not become unbound. If convective dredge-up can occur during the early phases of core He burning, the abundance of catalysts will rise in the surrounding hydrogen, thereby making H shell burning vigorous; the star would then be more like Population I than Population III as far as its shell source is concerned. Woosley and Weaver do find that the abundance of nitrogen does rise in their low-density envelope. (As we discuss in CBA, the release of heavy elements in a wind after dredge-up in stars that undergo complete collapse can be used to severely constrain the number of black holes that can be generated by such stars.) We do not yet know the extent to which the differences between the Woosley and Weaver results and ours are due to the treatment of time-dependent convection or to the differences between Population I and Population III evolution. Both calculations agree that a super-Eddington phenomenon does exist, with associated dynamical consequences. The final state of our 500 $M_\odot$ Population I star consists of an unbound expanding shell surrounding a remnant helium star.

© American Astronomical Society • Provided by the NASA Astrophysics Data System

1984ApJ...280..825B

f) The Helium Core Phase

Bare helium cores are also pulsationally unstable upon ignition of the 3α process provided their mass is in excess of

$$M_{\alpha p} \approx (13 + 120Z)(Y_T/0.75)^2\, M_\odot\,. \qquad (28)$$

This is a fit to the numerical results of Stothers and Simon (1970), which holds for metallicity Z in the Population I as well as in the Population III range (for which $M_{\alpha p} = 13\, M_\odot$, since $Y_T = 0.75$). In massive stars, the pulsational instability is usually assumed to be effectively damped by the large extended red giant envelopes surrounding the cores, so no evidence would be seen of the instability. This may also be true in VMOs if they could retain the supergiant envelopes which they formed after core hydrogen burning. However, since the coupling between core and envelope may be small for a very low density envelope of the sort found by Woosley and Weaver (1982), damping of core oscillations may be only partial. An oscillating helium core would undoubtedly result in mass loss, sending pure helium into the external medium in a wind. Convective cores tend to be quite large in these helium stars, over 90% by mass, so a large amount of loss in this phase will result in the escape of synthesized oxygen. Thus, if, say, more than 10% of the helium core's mass (~5% of the initial star's mass) escapes by this mechanism, it will be oxygen enriched, and this could be used to constrain the helium ejection during this phase by the metallicity arguments of the sort we discuss in CBA. However, since no work has been done on this phase, no reliable estimate can be given at this time of wind-ejected metallicity.

A VMO helium core can be modeled by an $n = 3$ polytrope. The polytropic mass is given by

$$M_{\alpha 3}(\sigma) = 9.9\sigma^{1/2}(1 + \sigma)^{3/2}\, M_\odot\,, \qquad (29)$$

where $Y_T = 0.75$ has been used. The helium pulsational boundary mass has $\bar{\sigma} = 0.50$ for $Z = 0$; the hydrogen boundary value has $\bar{\sigma} = 0.32$ for Population II metallicity. The photon entropy of the helium core must be related to its initial main-sequence value; for large VMOs, $\sigma_f/\sigma_i = (4Y_{Ti}/3)(2Y_{ei})^{-1/2} \sim 1.7$ in order to have $M_\alpha = M_i/(2Y_{ei})$.

The luminosity of the core is again nearly Eddington: $L \approx 2.4 \times 10^{38}(1 + \sigma^{-1})^{-1} M_\alpha/M_\odot$ ergs s^{-1}. From arguments similar to those in § IIc, we can infer that $f_{cc}(0)$ is nearly one. Since Y_e remains fixed throughout helium burning, the size of the convective core does not have to shrink to maintain the radiative output, and it remains near unity. Both aspects of convective core evolution during helium burning were discussed by Deinzer and Salpeter (1964).

The central temperature at which helium ignites can be determined by again equating the energy generation to the luminosity (Appendix B):

$$T_{\alpha c} \approx 18.3\left(\frac{\sigma^2}{1 + \sigma^{-1}}\right)^{0.039}\left(\frac{Y_T{}^2}{Y_e X_\alpha{}^3}\right)^{0.039} \text{keV}\,. \qquad (30)$$

For the $M_\alpha = 32\, M_\odot$ and $64\, M_\odot$ helium cores of Arnett (1973), we predict $\bar{\sigma} = 1.11$ and $T_{\alpha c} = 18.0$ keV, and $\bar{\sigma} = 1.84$ and $T_{\alpha c} = 18.8$ keV, respectively. He gets 17.9 and 18.9 keV. The El Eid, Fricke, and Ober (1983) $M_\alpha = 100\, M_\odot$ core is predicted to have $\bar{\sigma} = 2.46$ and $T_{\alpha c} = 19.3$ keV, which compares with their 19.2 keV.

g) The Mass Boundaries of VMOs

A quick and reasonably accurate estimate of the upper mass limit for VMOs can be obtained using the general relativistic polytropes explored by Tooper (1964) and Bludman (1973). The equation of state is assumed to be of form $p \sim \rho^{\Gamma_1}$, where ρ is the total mass-energy density and Γ_1 is constant. If, in addition, $p_c/\rho_c c^2$ is small, Bludman shows that such a polytrope configuration is unstable if

$$\Gamma_1 - \tfrac{4}{3} \leq 1.73 p_c/\rho_c c^2\,.$$

For VMOs, the ratio of radiation energy density to the baryon density—$3s_\gamma T/(4m_N) \sim 10^{-2}(M/10^6\, M_\odot)^{1/2}$ for main sequence VMOs—can be neglected; thus $p_c/\rho_c c^2 = Y_T(1 + \sigma)\, T_c/m_N$. If we now use equation (10a) in the large σ limit, we obtain an expression for the critical value of σ and of mass in terms of the central temperature:

$$(\Gamma_1 - \tfrac{4}{3})_{cr} = (6\sigma_{cr})^{-1} = 1.73\, Y_T\, \sigma_{cr}\, T_c/m_N\,,$$
$$M_{cr}(T_c) \approx 17.6 Y_T{}^2 \sigma_{cr}{}^2\, M_\odot = 1.6 \times 10^6 Y_T(1\,\text{keV}/T_c) M_\odot\,. \qquad (31)$$

The critical mass in the hydrogen-burning phase above which instability must occur can be estimated by substituting the equilibrium temperatures, equations (11a) and (11b), into this formula:

$$M_{cr} = 5.5 \times 10^5 (Y_T/1.7)^{1.03}(X_{CN}/10^{-2})^{0.052}\, M_\odot,$$

Population I and II; (32a)

$$M_{cr} = 1.7 \times 10^5 (Y_T/1.7)^{1.04}(X_{CN}/10^{-9})^{0.073}\, M_\odot,$$

Population III. (32b)

If we choose $X_{CN} \sim 10^{-4}$ as characteristic of Population II, we obtain $4.4 \times 10^5\, M_\odot$. Our simple estimates agree reasonably well with the results of Fricke (1973), who got $4 \times 10^5\, M_\odot$ for Population I abundances, and $10^5\, M_\odot$ for Population III. His inclusion of the kinetic energy gained during the prior collapse, which drives the star somewhat beyond stable equilibrium, results in his somewhat smaller values. Population III SMOs all collapse to black holes, even if they are slowly rotating (Fricke 1974). Fricke (1973, 1974) finds that Population I and II SMOs in a narrow mass range above M_{cr} can explode, but that large SMOs always form black holes. The thermonuclear behavior of rapidly rotating SMOs has not been explored sufficiently to determine their fate. Zel'dovich and Novikov (1971) estimated that if no nuclear burning were to intervene, a hydrogen star would suffer the general relativistic instability before the pair instability as long as $M > 6.4 \times 10^4\, M_\odot$. Our boundaries are well above this mass.

The corresponding critical mass for the helium-burning phase is obtained using equation (30) for the helium ignition temperature:

$$M_{\alpha,\,cr} = 4.7 \times 10^4\, M_\odot\,. \qquad (33)$$

Fricke (1973) gets $3.4 \times 10^4\, M_\odot$ for this mass. More massive cores will already be collapsing when they enter their oxygen core phase, and will end up as black holes. Their thermodynamic evolution is so similar to those stars which form stable oxygen cores and then go pair-unstable that we have included this range in the VMO definition.

© American Astronomical Society • Provided by the NASA Astrophysics Data System

1984ApJ...280..825B

For the lower mass boundary, we suppose that for oxygen core masses below 30 $M_\odot$, the star never goes pair-unstable. This is discussed more fully in the next section. The corresponding helium core mass is $\sim 35\ M_\odot$. Using the point source models and Figure 1, we then obtain $\sigma_c = 0.68$ and $M \sim 81\ M_\odot$. Weaver and Woosley (1980) have estimated that this lower boundary is significantly higher, $\sim 125\ M_\odot$. We attribute this discrepancy to the modifications which can occur in the quasi-static carbon burning portion of the evolution. We adopt $10^2\ M_\odot$ for the lower boundary ($M_O \approx 40\ M_\odot$).

III. VMO EVOLUTION IN THE OXYGEN CORE PHASE

In this section, we use simplified models to follow the oxygen core through to either collapse or explosion. In § III*a* an overview of the thermodynamic evolution is given. In § III*b* we set up a marginally stable model of an oxygen core, assuming its density structure is that of an $n = 3$ polytrope. In § III*c* we utilize a global effective potential, basically the core's binding energy, to study the evolution of a sequence of polytropic models of the collapsing core. The use of both polytropes and binding energy arguments in studies of the fates of massive objects is fairly common. In particular, Fowler and Hoyle (1964) used $n = 3$ polytropes to discuss the pair-instability supernova, which they introduced in their paper. Fowler (1966) studied the stability of Supermassive Objects via the binding energy approach. This method was extended by Zel'dovich and Novikov (1971), who calculated the mass boundary between those stars which first go pair-unstable and those that first encounter the general relativistic instability. (See § III*a* for a discussion.) Our extension allows nuclear burning to be included in the same sort of formalism. In § III*d*, the instantaneous nature of oxygen burning is expressed in terms of entropy jumps in the regions of the core which exceed an ignition temperature. In § III*e*, the breakup of heavy nuclei into α-particles is discussed. Our models are thus idealized to have three distinct phases: (1) onset of the pair instability; (2) oxygen burning; (3) alpha-quenching. The degree to which phase (3) occurs determines whether a black hole forms or not. In § III*f*, we estimate the critical core mass above which a black hole forms. The effects of slow rotation on this estimate are also discussed. In § III*g* we use entropic arguments to present the sequence of events which occur in the final stages of collapse to a black hole. In § III*h* we estimate the explosive energy released, and the fraction of oxygen burned in those VMOs which disrupt.

Here, we give a brief review of the older numerical calculations of oxygen core collapse. These experiments have concentrated on the low mass range, since one may expect that a few of these will be exploding in the present epoch. Fraley (1968) evolved 45, 52, and 60 $M_\odot$ cores. He found that the first did not explode, but oscillated, slowly consuming oxygen, while expelling only 1–2 $M_\odot$; the implication is that a massive black hole would be the final state. The other two stars exploded, perhaps resulting in complete disruption with no remnant left. Barkat, Rakavy, and Sack (1967) evolved 30 and 40 $M_\odot$ oxygen cores. The former entered into a relaxation oscillation phase fed by burning; it did not explode. The 40 $M_\odot$ core did explode. Arnett (1973) evolved 64 and 100 $M_\odot$ helium cores, corresponding to 58 and 93 $M_\odot$ oxygen cores; both exploded. The former left a loosely bound 2.2 $M_\odot$ silicon remnant whose fate was not determined. The 93 $M_\odot$ core completely disrupted. Wheeler (1977) evolved 10^3 and $10^4\ M_\odot$ oxygen cores, and in both cases found black holes were the final states, and no ejection of mass occurred. These numerical experiments agree on general trends: low masses oscillate without shedding much, if any, mass; intermediate masses completely disrupt, creating very energetic supernova explosions; high masses form black holes without ejection. The experiments obviously disagree on the detailed evolution of stars of the same mass.

a) Trajectory in Thermodynamic Phase Space

Rakavy and Shaviv (1968) recognized the utility of using the dimensionless entropy per baryon to characterize the collapse trajectory. We note that these authors do not properly zero their entropy, and the values we obtain differ from theirs by a constant 1.56. The entropy per baryon of the electron-positron plasma is now given not by the Sackur-Tetrode formula, but by the more general expression

$$s_e = (\epsilon_e + p_e/n_B - \mu_e Y_e)/T\ , \tag{34}$$

where ϵ_e and p_e are the e^+e^- internal energy per baryon and pressure, μ_e is the electron chemical potential, Y_e is the number of ionization electrons per baryon, n_B is the baryon density, and T is the temperature in energy units. The various terms in equation (34) must be evaluated numerically in the regime of concern to us, where the electrons and positrons are semirelativistic. To this is added the photon entropy, equation (6), and the nuclear entropy for an oxygen plasma,

$$s_N = Y_I \ln (T^{3/2}/\rho) + 1.61\ , \tag{35}$$

where $Y_I = 1/16$. Adiabats for pure oxygen plasmas in the ρ-T plane were computed numerically and are displayed in Figure 3, along with the pair instability region where the adiabatic index $\Gamma_1 < 4/3$. The lines for which the lifetime of an oxygen nucleus to react with another one is 10^4 s and 1 s are also shown. The rate was taken from Fowler, Caughlin, and Zimmerman (1975) (FCZ II). The trajectory of a mass element in thermodynamic phase space lies along an adiabat; burning on the 1 s time scale does not occur until after the element passes out of the instability region. However, it will overshoot this line as a result of the kinetic energy it gained while unstable. In this figure, we also show where the cores of stars of mass below the VMO boundary will lie at various burning stages. Presupernova II stars are presumably just those that skirt the e^+e^- instability region with $s < 8$. Oxygen and silicon can then be burned on relatively long time scales by stable stars, giving time for neutrinos to transport away not only energy but also entropy; as these stars evolve, the fusion of lower mass nuclei to higher mass ones results in a more ordered core in which the entropy progressively goes down. By the time an iron peak core forms, s has dropped to values in the center ranging from ~ 0.8 for $M \sim 25\ M_\odot$ up to ~ 2.2 for $M \sim 100\ M_\odot$; s has a positive gradient in the core due to differential energy losses via neutrinos.

We assume that each mass element of an oxygen core

© American Astronomical Society • Provided by the NASA Astrophysics Data System

1984ApJ...280..825B

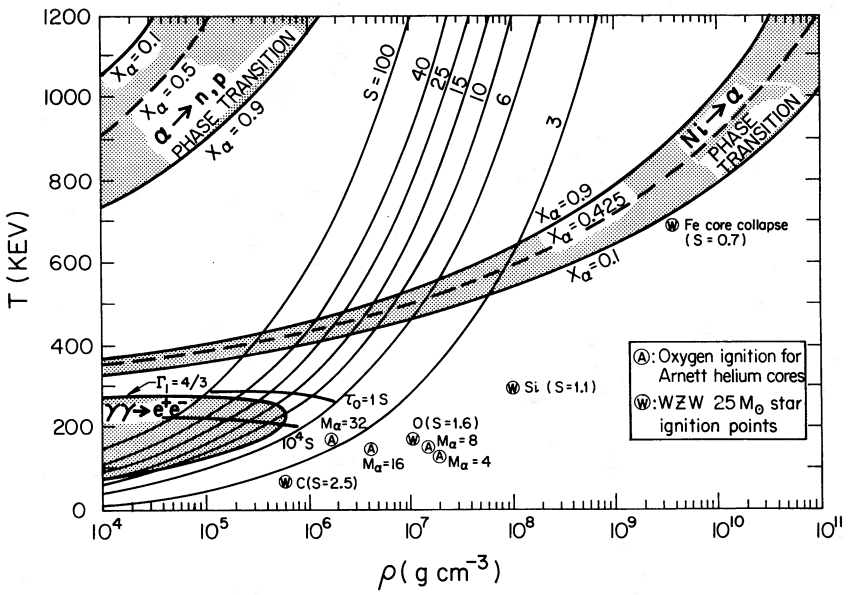

FIG. 3.—Isentropic lines for a plasma of oxygen nuclei and pairs are plotted in thermodynamic phase space, along with the various instability regions through which they pass. Lines of constant alpha abundance, X_α, through the nuclear phase transitions, lines where the oxygen burning lifetime, τ_O, is 1 s and 10^4 s, and points corresponding to Arnett's (1972) helium core calculations and Weaver, Zimmerman, and Woosley's (1978) 25 $M_\odot$ star calculations are also shown. The critical region for pair instability supernovae is $s \sim 8$–13.

with $M_O > 30\ M_\odot$ is approximately isentropic in time prior to the generation of entropy in the oxygen burning nuclear transmutations or its significant transport from the core by neutrinos. (The $e^+e^- \rightarrow \nu\bar{\nu}$ reaction rate becomes of the order of the dynamical collapse rate only much later in the evolution toward a black hole, as we shall show below.) During the "4α" process, the core is convective, and thus adiabatic. *The oxygen core is thus spatially as well as temporally isentropic.*

It is instructive to explicitly calculate the entropy required to make pairs when they are nonrelativistic ($T < m_e/3.15$). The number of nonrelativistic positrons per baryon is given by

$$Y_+ = \frac{3^4 5^2}{2^8 \pi^7} \frac{s_\gamma^2}{Y_e} \left(\frac{2m_e}{T}\right)^3 e^{-2m_e/T} \tag{36}$$

$$\approx 1.0 \times 10^{-3} \sigma^2 (T/100\ \mathrm{keV})^{7.2} \quad \text{near} \quad T \sim 100\ \mathrm{keV}.$$

The power law is accurate only in the neighborhood of $T = 100$ keV. Generally, $Y_+(\sigma, T) = Y_+(\sigma, T_0)(T/T_0)^{\nu_{pr}}$, where

$$\nu_{pr}(T) = 2m_e/T - 3\ . \tag{37}$$

The entropy in electrons and pairs is $s_e = s_e^{(0)} + s_{pr}$, where the pair entropy is given by

$$s_{pr} = Y_+(\nu_{pr} + 8.5)\ . \tag{38}$$

For example, at 100 keV, the entropy required to make an e^+e^- pair is 16. This entropy is primarily transferred from the photons, which directly robs the pressure.

We can again relate σ to the mass through the polytropic mass equation; for pure oxygen cores ($Y_T = 0.56$),

$$M_O = 5.6\sigma^{1/2}(1+\sigma)^{3/2}\ M_\odot\ . \tag{39}$$

Prior to pair production, the range of s_γ is thus ~4 to 100 for masses from ~30 to $10^4\ M_\odot$. We can also apply the formula for the critical mass above which the star is unstable due to general-relativistic effects, equation (31), to oxygen cores. If we take 100 keV as a typical central temperature above which the pair instability will be important for the entire core, then this gives a critical mass of 8000 $M_\odot$. A careful calculation of the mass boundary below which a core goes pair unstable first would have to include, for example, the mass dependence of the pair-unstable temperatire. Zel'dovich and Novikov (1971) obtained the value of 8000 $M_\odot$ for a core composed of iron. The value their method would give for oxygen cores should be only slightly higher.

Though the core mainly consists of oxygen, some carbon also exists. Prior to oxygen burning, carbon can ignite, producing neon and magnesium. Neon can then burn via an (α, γ) reaction. Both nuclear processes result in local entropy changes. If they occur quasi-statically, $\nu\bar{\nu}$ losses can be significant and lower the entropy. The result would be an entropy distribution which is a step function if the burning stages are convectively unstable, and a continuous distribution if the nuclear luminosity can be transported radiatively. Arnett (1973) finds the latter holds true for his $M_\alpha = 64\ M_\odot$ core. In either case, the entropy will be smaller in the central regions of the core than at the boundaries. Arnett's $M_\alpha = 100\ M_\odot$ core actually begins to collapse prior to carbon burning. In this case, the nuclear transmutations will add extra entropy to the central regions which burn first. We neglect the complications arising from these deviations from spatial adiabaticity, though we recognize they result in quantitative changes to the numbers we derive.

As we shall demonstrate, the evolution of the initially isentropic core in the thermodynamic phase space of Figure 3 proceeds as follows: All of the mass zones evolve along the same adiabatic track; they move slowly until the central

© American Astronomical Society • Provided by the NASA Astrophysics Data System

1984ApJ...280..825B

zone first reaches the $\gamma\gamma \rightarrow e^+e^-$ instability boundary. The core rapidly speeds up as it drops deeper and deeper into a self-generated effective potential well until the leading central zone crosses into the stable region. While still accelerating, these central zones encounter the oxygen ignition line ($T \sim 280$ keV), where they are transmuted to silicon and change tracks to a higher adiabat before the other zones can respond. The high-pressure inner zones would drive the core outward to low densities. However, the middle zones are still in the instability region and want to maintain their downward plunge. The core as a whole experiences a global deceleration, but is still moving to higher density due to the residual of the velocity it acquired upon infall while globally pair-unstable. The central zones may cross the silicon-to-nickel transmutation line ($T \sim 350$ keV), and even enter the nickel-into-alpha phase transition region to the alpha-quenching line ($T \sim 480$ keV) where all decelerating effects of the nuclear burnings are nullified. The initial entropy of the core determines whether the effective potential will rise to positive values and drive the entire core back out through lower densities, with the central zones traveling upon the higher adiabat tracks and the outer zones upon the original.

b) *The Polytropic Structure Approximation*

A spatially isentropic, chemically homogeneous structure which is in hydrostatic equilibrium may be calculated by the numerical solution of a second order ordinary differential equation (Poisson's equation), since the pressure depends only upon the density. Rakavy and Shaviv (1968) have utilized these structures in their study of oxygen cores. However, here we must explicitly consider dynamics of the core; during collapse, it passes through a series of shapes defined by the radius, $r(m, t)$, and density, $\rho(m, t)$, at time t as a function of the Lagrangian interior mass (i.e., baryon number) coordinate m, found by simultaneously solving the equations of motion and baryon conservation. As long as the central density, $\rho_c(t)$, is monotonically increasing, we can use it as our time variable. To get dimensionless equations, we define the following dimensionless quantities: $m_* = m/M$, with M the total mass; $\rho_* = \rho(m_*, \rho_c)/\rho_c$; $r_* = r/L$, with L given by $4\pi L^3/3 = 54.18M/\rho_c$. Isentropic core collapse is then defined by a smooth functional evolution in ρ_*-space. The simplest *a priori* assumption for this is that of homologous contraction in which the radius of the mass element labeled m satisfies $r(m, t) = a(t)r(m, t_0)/a(t_0)$, where $a(t)$ is a scale factor independent of m. In this case, the baryon density scales as a^{-3}, and ρ_* and r_* are t-independent. Generally, this assumption is valid only for $n = 3$ polytropic structures, although if the motion is sufficiently slow, arbitrary spatial structures can be treated. We approximate the functional evolution by $\rho_*(m_*, \rho_c) = \theta^3(m_*)$, where θ is the $n = 3$ Lane-Emden function; we expect the true solution to lie nearby in function space. Fowler (1966) and Zel'dovich and Novikov (1971) have repeatedly used this assumption in deriving relations for SMOs; we follow their lead to treat VMOs.

Near the global core instability point, defined by $\langle \Gamma_1 \rangle = 4/3$, where

$$\langle \Gamma_1 \rangle = \int \Gamma_1 p/\rho dm \Big/ \int p/\rho dm$$

is pressure-averaged, our $n = 3$ polytrope assumption will presumably be the closest to validity. Clearly, the zones within the pair instability region will be more tightly packed together than those outside; however, for both inside and outside zones, the deviations from the polytrope can be treated as perturbations. We define the mass at this point.

The polytropic mass (equation [8a]), $M_3(s, \rho_c) \sim (p_c/\rho_c{}^{4/3})^{3/2}$, depends upon the degree of central instability,

$$\frac{\partial \ln M_3}{\partial \ln \rho_c} = \frac{3}{2}\left(\Gamma_1 - \frac{4}{3}\right)_c ,$$

and thus varies during collapse. This equation explicitly shows the deviation of the equation of state from a $\Gamma_1 = 4/3$ law, and was used in Figure 3 to plot the pair instability boundary curve. In the regions where M_3 falls with increasing ρ_c, the center will be dynamically unstable, but the rest of the core with its spread of densities may not be: the polytropic mass depends not only upon time, but also upon the spatial Lagrangian point. Since the core mass is fixed, and the polytropic mass is not, we must present a prescription for the choice of mass: we fix M by requiring that the core be marginally stable when $\langle \Gamma_1 \rangle = 4/3$.

The global forces acting on the core are expressed by the mass-averaged first radial moment of the equation of motion, the virial equation for a sphere of mass M_s:

$$\int_0^{M_s} r\ddot{r} dm = W ; \tag{40}$$

$$W(\rho_c) = 3(\bar{P} - P_s)v + \Omega_G \tag{41}$$

is the "virial potential" evaluated for an $n = 3$ polytrope, where $\bar{P}v$ is the pressure volume-averaged over the sphere of volume v, $P_s = P(M_s)$, and

$$\Omega_G = -\int_0^{M_s} \frac{Gm}{r} dm$$

is the gravitational potential energy within the sphere. Since W obeys

$$\rho_c \frac{\partial W/\Omega_G}{\partial \rho_c} = \left\langle \Gamma_1 - \frac{4}{3} \right\rangle \frac{3\bar{P}v}{\Omega_G} - \left(\Gamma_{1s} - \frac{4}{3}\right)\frac{3P_s v}{\Omega_G} ,$$

if the surface term is negligible, our criterion for finding the core mass is to make $W = 0$ at the first extremum of W/Ω_G. At this point, the deviation in the value of W for the polytrope from its value for the true isentropic structure is essentially of second order ($O[(\Gamma_1 - 4/3)\delta r]$); we may therefore expect M so obtained to be a reasonable estimate of the true value. In practice, we include the surface terms in order to treat various inner core sizes; later we extend this to deal with shells. Our global core calculations actually refer to the inner 97% by mass (r_* is only 0.61), and the mass definition naturally includes the small surface term since it contributes to the global instability. The fit

$$M_O(s) = 56(s/10)^{2.5}\, M_\odot \tag{42}$$

is very accurate over the $8 < s < 15$ range of primary interest to us. In Figure 4, we plot $(-W/\Omega_G)$ for given s. This quantity, which is initially zero, goes negative as the pair instability region is entered, and maintains negative values even after this region is traversed (in the absence of nuclear burning), which reflects the fact that the creation of the pair

© American Astronomical Society • Provided by the NASA Astrophysics Data System

1984ApJ...280..825B

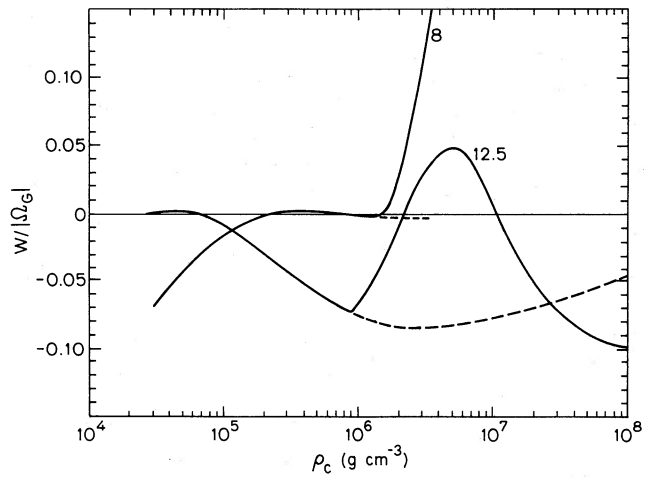

FIG. 4.—The ratio of the virial potential to the gravitational potential energy is plotted against central density for oxygen cores with the initial entropies $s_i = 8$ and 12.5. The former is just marginally unstable to the pair instability; the latter is violently unstable. The dashed line would give the evolution if there were no nuclear burning.

degrees of freedom from the photons results in a net loss of pressure, even though the $\Gamma_1 > 4/3$ state is regained; the small amount of ionic pressure still present is responsible for the increase in $(-W/\Omega_G)$. In the asymptotic limit, the pairs become extremely relativistic, $s_e \to 7s_\gamma/4$, and the polytropic mass approaches $M_{er} = 0.66(s_{er})^2(1 + 4Y_I/s_{er})^{3/2} M_\odot$, where $s_{er} = s_e + s_\gamma$ very slowly approaches $s - 1.61$; here we have used equations (8a) and (35). This mass is substantially below the mass we compute according to the $W = 0$ prescription, which reflects the relative pressure loss due to pair creation.

If the core were homologously infalling, it would do so on the dynamical time scale

$$\tau_{dyn} = (\Omega_G/W)^{1/2}\tau_{ff}; \quad (43)$$
$$\tau_{ff} = (2|\Omega_G|/I)^{-1/2} \approx 2.6(10^6/\rho_c)^{1/2} \text{ s}$$

is the free-fall time, where I is the spherical moment of inertia. Thus, for the $s = 13$ core, the dynamical time at 10^6 g cm^{-3} is predicted to be 10 s, elongated by a factor of ~ 4 from free fall. It is thus only $\sim 10\%$ out of pressure balance and never gets appreciably more than this: the pair instability is not a violent one, unlike the nuclear phase transitions we meet later.

c) The Effective Potential

The virial potential tells only of the accelerating and decelerating forces acting on the core; the kinetic energy is related to the integral of W with respect to the logarithm of the central density for homologous collapse. More generally, the kinetic energy of the sphere changes according to the global energy conservation equation: $d(K + V)/dt + P_s\, dv/dt + L = 0$. Here, L is the luminosity due to $\nu\bar{\nu}$ pairs which we can neglect, and

$$V(\rho_c) = \int_0^{M_s} (\epsilon_\gamma + \epsilon_e + \epsilon_I + \epsilon_{nuc} - Gm/r)dm \quad (44)$$

is the sum of the internal, nuclear, and gravitational energies stored within the core of radius M_s. If we know the time history of the surface pressure, then we can form an effective potential energy

$$V_e(\rho_c) = V(\rho_c) - V(\rho_{c0}) - \int_0^{M_s} dm \int_{\rho_{c0}}^{\rho_c} p_s(M_s, \rho_c)/\rho(m, \rho_c)d\rho_c/\rho_c \quad (45a)$$

$$= \tfrac{1}{3}\int_{\rho_{c0}}^{\rho_c} W(\rho_c)d\rho_c/\rho_c\,. \quad (45b)$$

In collapses without energy loss, $K + V_e$ is constant; if at the point of global instability we assume $K = 0$, then $K = -V_e$, where the conserved total energy has been arbitrarily normalized to zero. Equation (45b) holds exactly for homologous collapse, even if nuclear burning occurs. As evolution proceeds further into the instability region, V_e becomes progressively more negative. Without nuclear burning, $V_e/\Omega_G \to$ constant, since the internal energy scales the same way as the gravitational energy as $\Gamma_1 \to 4/3$. The inclusion of nuclear burning causes V_e to become less negative; if it goes to zero again, then we can infer the core collapse halts, and the flow becomes outward directed. Figures 5 and 6 show how the inclusion of nuclear burning (according to the prescription of the next section) and alpha-quenching (as described in § III*e*) changes the effective potential. We extend the potentials into the positive regime, although this region is predicted to be inaccessible to the core. We shall see that, if turnaround can occur, then explosive disruption will almost certainly follow: since the explosion trajectory of the central zones is on a higher adiabat, there is more pressure than was there during infall, which was itself marginally stable.

d) The Instantaneous Burn Approximation

The lifetime for an oxygen nucleus to undergo a nuclear transmutation with another oxygen nucleus in the plasma, τ_O, is given by FCZ II; their expression was used to construct the $\tau_O = 10^4$ and 1 s lines of Figure 3. If we define the index $\nu(T)$ as $(\partial \ln \tau_O/\partial \ln T)_\rho$, which is thus density independent, we find $\nu(280 \text{ keV}) = 24.8$; in the neighborhood of this temperature, $\tau_O \approx 0.7\rho_5^{-1}(280/T)^{24.8}$ s. Even at this relatively high temperature, the burning rate is extremely temperature sensitive; thus, the 1 s burn line has almost no density sensitivity. Since a typical dynamical time for the core is 10 s at 10^6 g cm^{-3}, the concept of an ignition temperature, T_{ign}, is appropriate: When the temperature is below T_{ign}, the burn time is much greater than the dynamical time; when above it, much smaller. We take T_{ign} for oxygen burning to be 280 keV, assuming it to be independent of density over the region of interest.

The immediate products of oxygen burning are silicon and sulfur. At a higher temperature, silicon burning occurs and these products themselves transmute via the usual breakdown-buildup process to iron peak elements. We suppose for simplicity that burning occurs in two phases: O→Si→Ni, which releases 471.5 keV in the first stage and 195 keV in the second stage; we assume the latter occurs at its own $T_{ign} = 350$ keV, chosen on the basis of the ^{24}Mg(γ, α) and ^{28}Si(γ, α) lifetimes given in FCZ II. Silicon burning should,

© American Astronomical Society • Provided by the NASA Astrophysics Data System

1984ApJ...280..825B

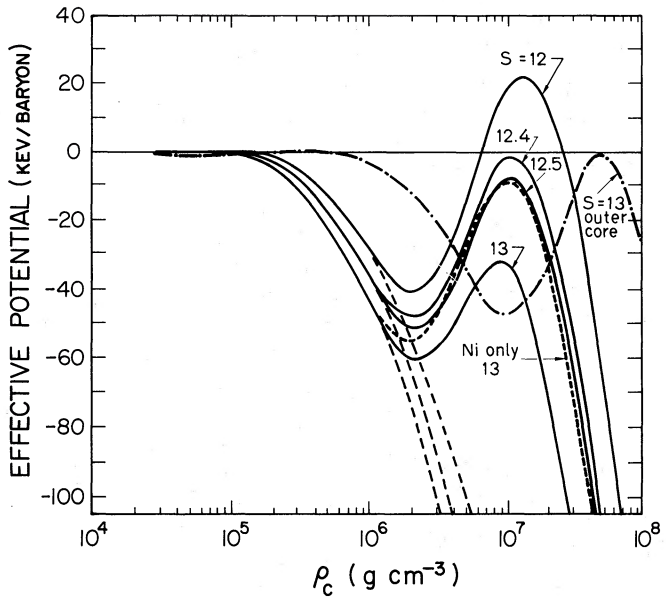

FIG. 5.—The effective potential (per baryon) is plotted for a sequence of $n = 3$ polytropic density structures, labeled by the central density ρ_c. Its value should be compared with the gravitational potential per baryon, $\Omega_G = -1500\,(M_O/100\,M_\odot)^{2/3}(\rho_c/10^6\,\mathrm{g\,cm^{-3}})^{1/3}$ keV. The three regimes of pair instability, oxygen burning, and alpha-quenching are apparent. The $s_i = 12$ core explodes; the rest collapse to black holes. The long dashed curves are evolutions with no oxygen burning. The short dashed curve for $s_i = 13$ has oxygen transmuted to nickel directly rather than through an intermediate silicon phase. The dash-dot curve shows the effective potential for just the outer one-third of the $s_i = 13$ core.

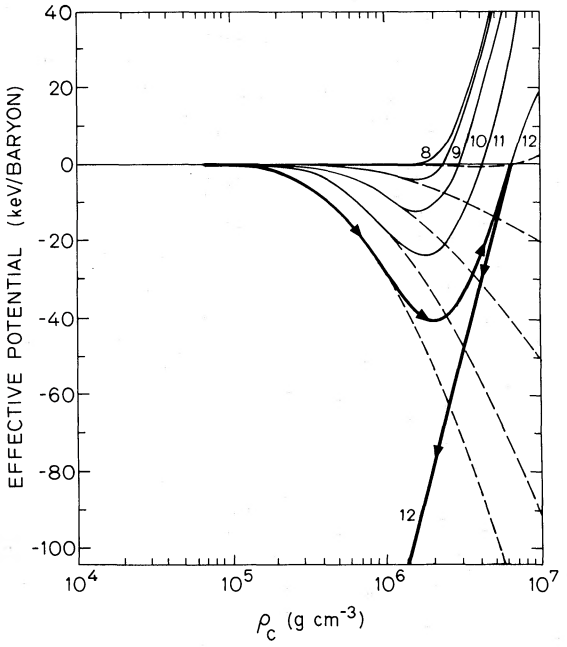

FIG. 6.—Same as Fig. 5, but for those oxygen cores which explode. Once the effective potential reaches zero, implosion stops and the core expands following a steeply dropping effective potential drawn explicitly for the $s_i = 12$, $M_O \approx 90\,M_\odot$ case.

of course, be treated with a large network since the passage to Ni is achieved through a series of quasi-equilibrium clusters in the (N, Z)-plane of nuclei (Bodansky, Clayton, and Fowler 1968; Woosley, Arnett, and Clayton 1973). We are unable with our crude approximation to make any statement about relative abundances of detailed nuclei. However, our results should reflect the relative abundances of oxygen and silicon burning products compared with oxygen in a VMO explosion.

Since the number of ionization electrons, Y_e, is 0.5, Ni might be expected to be the preferred nucleus in a nuclear statistical equilibrium (NSE) mix. Oxygen burning occurs so quickly that there is no time for electron captures and β-decays to change the neutron excess to any appreciable extent; this contrasts with the case of massive stars, where oxygen is burned over much longer time scales and a sizeable neutron excess can be built up by the time NSE is achieved (Weaver and Woosley 1980). Under the high entropy conditions operative in VMOs, other iron peak nuclei could dominate the NSE mix. The energetics of the explosion are somewhat dependent upon our choice of reaction pathway, which we have varied to demonstrate the sensitivity to the nuclear burning approximations. For example, we have considered the two phases to be O→S→Ni, with sulfur rather than silicon as the intermediate phase, and obtained similar results. We have also studied how the results change if burning occurs in one stage, O → Ni, at 280 keV; in this case, the black hole formation boundary only changes from initial entropy 12.4 to 13.

Consider a mass element which has passed through the instability region of Figure 3 and therefore gained kinetic energy. It approaches the ignition temperature along an isentropic trajectory, and reaches it at an ignition density $\rho_{\mathrm{ign}} = \rho(T_{\mathrm{ign}}, s)$. We now make the *instantaneous burn approximation*: before ρ changes significantly, either because of continued compression (governed by the dynamical time) or because of significant PdV expansion (governed by the sound crossing time τ_s), the nuclear transformation is essentially complete: $\tau_O < \min(\tau_{\mathrm{dyn}}, \tau_S)$. If so, the transition occurs at constant density and hence at constant energy (thermal plus nuclear) since there is then no PdV work. The entropy does change, by an amount $\Delta s(s; \mathrm{O}\rightarrow\mathrm{Si})$ given by

$$(\epsilon_e + \epsilon_\gamma + \epsilon_I)(s + \Delta s, \rho_{\mathrm{ign}}) = (\epsilon_e + \epsilon_\gamma + \epsilon_I)(s, \rho_{\mathrm{ign}}) + 471.5\ \mathrm{keV}\ , \tag{46}$$

where the ionic thermal energy per baryon, $\epsilon_I = (3/2)Y_I T$, has $Y_I = 1/16$ on the right-hand side and $Y_I = 1/28$ on the left. The pair energy ϵ_e contains the rest-mass energy. This Δs is precisely the value which would be obtained from the more direct calculation:

$$\Delta s = \int \dot{q}_{\mathrm{nuc}}/T\,dt - \int (\mu_O\,\dot{Y}_O/T + \mu_{Si}\,\dot{Y}_{Si}/T)dt\ ,$$

where $\dot{q}_{\mathrm{nuc}}$ is the rate of nuclear energy release, Y_O is the number of oxygen nuclei per baryon at time t, and μ_O is the chemical potential (excluding the nuclear rest mass term which has been absorbed into $\dot{q}_{\mathrm{nuc}}$). The nuclear entropy change, Δs_N, is actually negative, since although there is a higher temperature, the freezing out of nuclear degrees of freedom due to the buildup of more complex nuclei from lighter ones overcomes this: $\Delta s_N \approx -0.5$ (cf. $s_O \approx 1.3$). This is compensated by the entropy change in photons and pairs: $\Delta(s_e + s_\gamma) \approx 1.7$

© American Astronomical Society • Provided by the NASA Astrophysics Data System

1984ApJ...280..825B

(cf. $[s_e + s_\gamma] \approx 9.7$). For this $s = 11$ example, the temperature jumps 15 keV in the transmutation. We find the following fit to the solution to equation (46) to be adequate:

$$\Delta s(s; \mathrm{O} \rightarrow \mathrm{Si}) = 1.187, \quad s > 15,$$
$$= 1.185 + 0.0015(s-12) - 2.78 \times 10^{-4}(s-12)^2, \quad 8.5 < s < 15,$$
$$= 1.165 + 7.33 \times 10^{-3}(s-7), \quad 6.5 < s < 8.5. \tag{47}$$

We calculate the further change in entropy due to the Si→Ni transition by using equation (46), with the starting entropy now $s + \Delta s(\mathrm{O} \rightarrow \mathrm{Si})$:

$$\Delta s[s + \Delta s(s, \mathrm{O} \rightarrow \mathrm{Si}); \mathrm{Si} \rightarrow \mathrm{Ni}] = 0.25 + 5 \times 10^{-4}(s-20), \quad s > 14,$$
$$= 0.247, \quad s < 14. \tag{48}$$

Thus the $s = 14$ trajectory first changes by 1.19 in oxygen burning, then by 0.25 in silicon burning to make the total change 1.44; if sulfur is the intermediate nucleus, the changes are 1.26 + 0.20 = 1.46; if oxygen is immediately transmuted to nickel at 280 keV, the change is still only 1.51.

e) *Alpha-Quenching*

As the temperature rises, we assume NSE sets in with nickel being the most abundant nucleus. This is consistent with our simplified α-particle nuclei picture of burning which we suppose is maintained in the nickel-into-alpha phase transition. This is not quite true, since other nuclei become abundant before this transition is met (Bodansky, Clayton, and Fowler 1968). The Ni→α transition conserves entropy since it occurs in equilibrium among the nuclear species. The balancing of chemical potentials and binding energies leads to a polynomial of order 14, expressing baryon number conservation, which determines the alpha abundance. X_α is found to change gradually from 0.1 to 0.9 over a temperature range of 70 keV for the entropies of interest.

The nuclear potential energy gained due to oxygen and silicon burning is lost at the alpha-quenching boundary, defined by $\epsilon_{\mathrm{nuc}}(\mathrm{Ni} + \alpha) = \epsilon_{\mathrm{nuc}}(^{16}\mathrm{O})$, which occurs when $X_\alpha = 0.425$. The passage from nickel to alpha costs 1589 keV per baryon, which is much larger than the 667 keV per baryon gained in nuclear burning. The alpha-quenching boundary is only indicative of the point at which the explosive effects of nuclear burning will be undone. Entropy is transferred from the photons and pairs to dissociate the α-particles from the heavy nuclei: nuclear degrees of freedom are liberated at the expense of relativistic thermal pressure $[= n_B(s_\gamma + s_e)T/4]$. The devastating effect on the entropy generation is illustrated in Figure 7 for an initial $s = 13$: s_N is initially 1.45, drops to even lower values after burning, then rises to 3.5 due to alpha-quenching; $s_\gamma + s_e$ suffers a corresponding drop. As more and more central zones cross the quenching boundary, the effective potential is driven down to more negative values (Fig. 5). If V_e is negative when alpha-quenching sets in, collapse will continue.

The next boundary to be crossed is the $\alpha \rightarrow 2n + 2p$ phase transition, which does not occur until the temperatures are in the MeV range: the transition region is displayed in Figure 3 for very high entropies. This transition costs

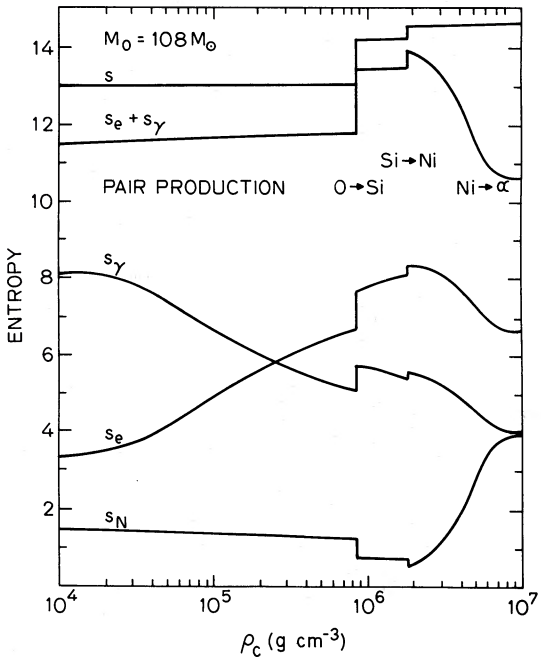

FIG. 7.—The entropy evolution at the center of the $s_i = 13$, $M_O = 110\ M_\odot$ oxygen core demonstrates the entropy input due to nuclear burning, and the entropy redistribution due to the pair instability and alpha-quenching.

7070 keV per baryon of nuclear potential energy and results in an even more substantial shift of entropy from relativistic particles to nuclear particles than in the Ni→α transition. The effective potential thus plunges toward its free-fall value, the gravitational potential energy.

f) *The Critical Mass for Black Hole Formation*

In our simple model, the global effective potential remains negative if $s > s_c \approx 12.4$ and becomes positive if $s < s_c$, as can be seen in Figures 5 and 6. The critical oxygen core mass is $M_{Oc} = M_O(s_c) \approx 10^2\ M_\odot$. The core is predicted to become globally unstable at $\rho_{c0} \sim 4 \times 10^4$ g cm^{-3}, as is demonstrated by the plot of $W/|\Omega_G|$ in Figure 3. The mass is determined at this point by setting $W = 0$. When the center of the core reaches $\rho_c \sim 10^6$ g cm^{-3}, the oxygen is predicted to ignite. An immediate effect can be seen in the virial potential, but the response of the effective potential is slower. Beyond $\rho_c \sim 2.5 \times 10^6$ g cm^{-3}, the core is globally decelerated due to the extra pressure generated by the nuclear energy input. In particular, this added pressure will cause a restructuring of the density profile: the center will have a lower density than that predicted by the polytrope approximation, and thus a lower temperature. This results in two important phenomena which limit the accuracy of our results: (1) Silicon ignition is delayed until later than the time it is predicted to occur in our models. This means that explosions will have fewer silicon-burning products than we predict. (2) Alpha-quenching is also delayed until later than predicted. By forcing the central density to be given by a polytrope, the devastating effects of the photodissociation of iron peak nuclei in the central regions drive the effective potential down before the full explosive effects of nuclear burning in the outer regions can be realized. This effect can be

© American Astronomical Society • Provided by the NASA Astrophysics Data System

1984ApJ...280..825B

seen in the drop in the virial potential (Fig. 4) beyond $\rho_c \sim 5 \times 10^6$ g cm^{-3}; by 10^7 g cm^{-3}, global inward acceleration once again resumes. The effective potential (Fig. 5) thus turns over at $\rho_c \sim 10^7$ g cm^{-3}. Our values of s_c and $M_{\rm Oc}$ are therefore underestimates.

If we supposed the one-stage burning transformation O → Ni to be operative, then the $s = 12.4$ core would be predicted to turn around. As can be seen in Figure 5, the increase in the $s = 13$ effective potential due to one-stage burning raises it to only the $s = 12.5$ two-stage burning peak which is negative and hence collapse is predicted. Uncertainties in the reaction pathway could therefore lead to errors of $\sim 10\ M_\odot$ in $M_{\rm Oc}$.

It may be argued that the regions which undergo quenching will collapse and those that do not will explode, resulting in black hole formation accompanied by metal ejection even if $M_{\rm O} > M_{\rm Oc}$. We can answer this objection by considering the energetics of a shell rather than of the entire core. The effective potential for a shell of interior mass m_1 and exterior mass m_2, $V_e(m_2, m_1)$, is simply the difference between the effective potentials of the larger and smaller spherical cores with the boundary terms appropriately included: $V_e(m_2, m_1) = V_e(m_2, 0) - V_e(m_1, 0)$. In Figure 5, the effective potential for the outer one-third ($m_{*1} = 0.678, m_{*2} = 0.968$) of the polytropic core for $s = 13$ is plotted. The onset of the pair instability and that of nuclear burning clearly occur in the shell when the central density is higher than for the entire core. Hence, though the shape of the effective potential is similar, the features are shifted. The outer core is predicted to collapse (marginally) and to follow the inner core toward its singular final state. Smaller entropy outer shells would be predicted to explode and larger ones to collapse.

The shell calculation has one advantage over the global calculation: it is not as sensitive to the deviations of the central structure from the $n = 3$ polytrope. The behavior of the outer shell is determined by the inner surface pressure, which drives explosion, as well as by the shell-averaged pressure forces, which also drive explosion, and the outer surface pressure and the gravitational potential of the shell, which drive collapse. Alpha-quenching in the inner core lowers this inner surface pressure, thereby ensuring outer core collapse in spite of the nuclear energy release there. (We cannot take the shell to be too small or else the differences between the true hydrodynamical and assumed profiles will not be smoothed over and the inner and outer pressures will be inaccurate.) We can conclude from these outer shell calculations that our global value for s_c is an underestimate ($s_c \sim 13$ is favored, which gives $M_{\rm Oc} \sim 110\ M_\odot$), but it is not wildly in error.

We can also investigate the sensitivity of our results to the addition of slow rotation, following the method used by Fowler (1966) and Fricke (1974). The rotational kinetic energy, K_R, adds an extra term to our effective potential: $V_{eR} = V_e + K_R$. For uniform rotation, $K_R = I\omega^2/3$, where I is the spherical moment of inertia and $\omega(t)$ is the uniform angular frequency. If the angular momentum, $J = 2I\omega/3$, is assumed to be conserved during collapse, then

$$V_{eR} = V_e - \tfrac{1}{2}\epsilon_{R0}\,\Omega_G(\rho_c/\rho_{c0})^{1/3}\ ,$$

where

$$\epsilon_R = 2K_R/|\Omega_G| = \tfrac{3}{2}J^2(|\Omega_G|I)^{-1}$$

measures the contribution of rotational energy to the pressure balance ($W_R = W - \epsilon_R\Omega_G$); ϵ_{R0} is its value at the onset of instability at ρ_{c0}. For slow rotation, ϵ_R has the same density dependence as the pressure contribution of a $\gamma = 5/3$ gas and thus becomes progressively more important as collapse proceeds.

Small rotation will increase the core mass we get for a given entropy due to the added rotational stability; at $\rho_{c0}(s, J)$, where $[\rho_c\,\partial(W_R/\Omega_G)/\partial\rho_c] = 0$, we obtain the mass from $W_R = 0$: $M(s, J) = M(s, 0)[1 + 3/2(J/J_0)^2]$ for small J/J_0. We have defined the breakup angular momentum, $J_0(M)$, by $\epsilon_{R0} = 1$; for the $s = 12.5$ core its value is $J_0/M \approx 10^{19}$ cm^2 s^{-1}. The specific angular momentum of a typical O5 star is at most $\sim 10^{18}$ cm^2 s^{-1}; $\epsilon_{R0} = (J/J_0)^2$ would likely be less than a percent. In order for rotation to cause the $s = 13$ effective potential to rise to zero in Figure 4, we need $K_R = 30$ keV per baryon at $\rho_c \sim 10^7$ g cm^{-3} which requires $J/J_0 \approx 0.2$. The modification of the critical entropy and mass is (for small J/J_0):

$$s_c(J) = s_c(0)[1 + a_s(J/J_0)^2], \qquad a_s \approx 1.4; \tag{49a}$$

$$M_{\rm Oc}(J) = M_{\rm Oc}(0)[1 + a_M(J/J_0)^2], \quad a_M \approx 3.5\ . \tag{49b}$$

Notice that $a_s \approx 0.4a_M$ follows from our approximate $M_{\rm O}(s)$ relation.

The critical mass is apparently not too sensitive to the amount of rotation according to equation (49). This is misleading for a number of reasons. First, if J is large enough that $\epsilon_R \sim 0.1$ during nuclear burning, then the rotational support can increase $\tau_{\rm dyn}$ sufficiently to make burning appreciable in regions with $T < T_{\rm ign}$, thus making explosion more likely. The clean separation of global collapse from explosion could also cease to hold with rotation: the Fowler and Hoyle (1964) picture of mantle explosion driven by a combination of rotational braking and oxygen burning may result. Even if a core continues collapsing after oxygen burning, rotation will play an increasingly important role as collapse proceeds since ϵ_R rises and large deviations from sphericity occur. If $J/J_0 = 0.2$, the core would be predicted to reach breakup speed by the time its radius has contracted by a factor of 25 from its value at the onset of instability. This would happen before the Schwarzschild radius is reached. When $\epsilon_R = 0.14$, the core goes secularly unstable and breaks its axial symmetry by populating azimuthally asymmetric modes according to the analysis of rigidly rotating $n = 3$ polytropes given by Bodenheimer and Ostriker (1973). If we naively force our core to follow a Newtonian polytrope profile, we would predict that a trapped surface would first form around $r_* \sim 0.4$ when the central density is $\rho_{cb} \sim 10^{13}(M_{\rm O}/100\ M_\odot)^{-2}$ g cm^{-3}. To avoid breakup, we would require $J/J_0(M) < 0.04(M_{\rm O}/100\ M_\odot)^{1/3}$. This crude argument illustrates that, if a VMO starts with a specific angular momentum similar to that of a main-sequence O5 star, and if it does not lose a significant fraction of it during its evolution, then, though thermonuclear explosion may be avoided, rotational effects could allow metal ejection during the catastrophic final collapse. A large emission of gravitational radiation could accompany such an asymmetric collapse. Clearly, large angular momentum collapses require further investigation.

© American Astronomical Society • Provided by the NASA Astrophysics Data System

1984ApJ...280..825B

g) Collapse to a Black Hole: Neutrino and Gravitational Wave Losses

Oxygen and silicon burning cannot turn implosion into explosion if $M_O > M_{Oc}$, and since all subsequent transmutations are endothermic, complete gravitational collapse to the black hole state will follow, at least if the spin of the core is not too large. By the time alpha-quenching onsets, the positrons and electrons are extremely relativistic and their entropy is given exactly by

$$s_e = \tfrac{7}{4} s_\gamma [1 + 15\eta^2 (7\pi^2)^{-1}] ; \qquad (50)$$
$$\eta + \eta^3/\pi^2 = (4\pi^2/15) Y_e/s_\gamma$$

relates the degeneracy parameter $\eta = \mu_e/T$ to the photon entropy and $Y_e = Y_{e^-} - Y_{e^+}$. These expressions give the extremely degenerate electron gas result $s_e = [(15\pi^2/4) Y_e^2 s_\gamma]^{1/3}$ as well as the high temperature limit when s_γ is large:

$$s_e = \tfrac{7}{4} s_\gamma [1 + (4\pi^2/105)(2Ye)^2/{s_\gamma}^2] .$$

As long as $s_\gamma > 1.9 (\eta < 0.68)$, the error in assuming $s_e \approx (7/4) s_\gamma$ is less than 10%; hence $s_{er} \approx (11/4) s_\gamma$ gives the entropy in relativistic particles. The nuclear entropy for a pure alpha gas is then

$$s_\alpha = 2.8 + \tfrac{1}{8} \ln (s_{er}/\rho_{10}) ,$$

where $\rho_{10} = \rho/(10^{10}$ g cm$^{-3})$; by 10^7 g cm^{-3} the phase transition to alphas is complete for the conditions of Figure 7 ($s \approx 14.5$), hence the nuclear entropy agrees with equation (51).

At this point neutrino losses can no longer be ignored. As long as neutrinos can freely stream from the core, the reactions $e^+ e^- \rightarrow \nu_e \bar{\nu}_e$, $\nu_\mu \bar{\nu}_\mu$, $\nu_\tau \bar{\nu}_\tau$ lower the entropy at a rate (assuming the Weinberg-Salam model of electroweak interactions with $\sin^2 \theta_W = 0.2$)

$$(-\dot{s})_{pair} \approx 364 {\rho_{10}}^{5/3} (s_{er}/10)^{8/3} \text{ s}^{-1} , \qquad (52)$$

which holds as long as η is small. In a homologous collapse, the density evolution follows

$$\dot{\rho}/\rho = 3[(-2V_e/I)]^{1/2} = 3(\chi \tau_{ff})^{-1}$$

where the free-fall time is given by equation (43) and $\chi = (V_e/\Omega_G)^{-1/2}$ measures the elongation of the dynamical collapse time over the free-fall time due to the pressure forces. Adopting this law, we obtain

$$n_s(\rho_c) \equiv -\frac{d \ln s}{d \ln \rho_c} \approx 0.55 \chi {\rho_{c10}}^{7/6} \left(\frac{s_{er}}{10}\right)^{8/3} \left(\frac{s}{10}\right)^{-1} . \qquad (53)$$

Thus entropy depends only weakly upon the density until the density is high. If we assume that $ds \approx ds_{er}$, which is reasonable since s_N depends only logarithmically on s_{er} and ρ provided nuclear transmutation is not taking place, then we can relate the relativistic entropy s_{er}' at density ρ_c' to its value, s_{er}, at the central density ρ_c assuming χ is approximately constant over this range:

$$s_{er}'/s_{er} = [1 + 10/7 (s' n_s'/s_{er}' - s n_s/s_{er})]^{-3/5} . \qquad (54)$$

This formula is not accurate unless pairs are relativistic; however, since it gives an overestimate of the role of pair neutrino losses in the semirelativistic regime, we can use it for the purposes of discussion.

It is clear that, if $\rho_c \sim 10^6$ g cm^{-3}, $n_s \sim 10^{-5} \chi$ is very tiny for $\chi \sim 5$, its value at the onset of oxygen burning for the $s = 13$ collapse. Therefore, over the range 10^4–10^8 g cm^{-3} when the VMO fate is decided, $\nu\bar{\nu}$ losses can be ignored, a result we have already invoked. If carbon burns prior to the onset of instability, evolution is quasi-static and χ can be very large, hence our initial collapse configuration may be not quite spatially isentropic.

It is not until $\rho_{10} \sim 1$, and therefore $T = 5.8 (\rho_{10} s_{er}/10)^{1/3}$ MeV, that $n_s \sim 1$ and $\nu\bar{\nu}$ losses significantly rob the core of entropy. Though $\chi (\rho_c \approx 10^8$ g cm$^{-3})$ is still 4.6 for the $s_i = 13$ collapse, which is rather far from free fall in the by now alpha-dominated core, once $\nu\bar{\nu}$ losses occur and s_{er} drops, the core becomes closer to free fall since $\chi^2 - 1 \sim {s_{er}}^{4/3}$. The $\alpha \rightarrow n, p$ transition, which does not occur until $T > 5$ MeV and $\rho_{10} \sim 1$ for $s_{er} \sim 10$, ultimately accelerates χ's approach to one.

The nuclear entropy of the free nucleon gas obeys

$$s_{np} = 8.7 + 0.5 \ln (s_{er}) - 0.5 \ln (\rho_{10}) , \qquad (55)$$

which is of order 10. If $s = 15$, which is ncar the critical entropy cut, the relativistic particles have less entropy than the free nucleons. The emission is correspondingly cut down, but $e^+ e^- \rightarrow \nu\bar{\nu}$ is now augmented by the Urca reactions $e^+ n \rightarrow \bar{\nu}_e p$, $e^- p \rightarrow \nu_e n$: these dominate the entropy loss for all but the most massive collapsing VMOs since

$$(-\dot{s})_{Urca} = (86/s_{er})(-\dot{s})_{pair} \qquad (56)$$

for $T \gg 1.3$ MeV.

The neutrino emission predicted by equations (52) and (56) is enormous before a trapped surface forms when $\rho_c \sim 10^{13} (M_O/100\, M_\odot)^{-2}$ g cm^{-3}. However, before this, neutrinos become optically thick due to the reactions $\bar{\nu}_e p \rightarrow e^+ n$, $\nu_e n \rightarrow e^- p$, $\nu e^\pm \rightarrow \nu e^\pm$, and later to $\nu\bar{\nu} \rightarrow e^+ e^-$, $\nu\bar{\nu}$ and $\nu\nu \rightarrow \nu\nu$. Muon and tau neutrinos do not participate in the inverse Urca reactions, but do participate in the others: their flow from the core is also impeded. An equilibrium mixture of neutrinos of all types, each with approximately zero chemical potential, forms in the core; thus "blackbody" radiation occurs from a neutrino photosphere, with volume emissivity occurring outside it. We term such a configuration a *neutrino fireball.*

The development of the fireball proceeds as follows. Just as in iron core collapse in massive stars, some neutrinos become trapped by their interactions with the imploding core and cannot escape. At late times, our VMO core then consists of neutrinos trapped and imploding in the center, surrounded by a shell of neutrinos diffusively outflowing, radiating as a fermionic blackbody from the neutrino photosphere with luminosity

$$L = (3 \times 2 \times \tfrac{7}{16}) 4\pi R^2 (\pi^2 T^4/60)$$
$$= 10^{58} {r_{*p}}^2 (T/5 \text{ MeV})^4 (M_O/100\, M_\odot)^{2/3} {\rho_{c10}}^{-2/3} \text{ ergs s}^{-1} . \qquad (57)$$

This is 21/8 times the usual photon luminosity expression: the factor of 3 comes from assuming three flavors of neutrinos, the 2 counts neutrinos and antineutrinos, and 7/16 is a factor arising from the difference between Fermi and Bose statistics. Equation (57) assumes that the ν_μ and ν_τ photospheres coincide with the position of the ν_e photosphere. In fact, since the

© American Astronomical Society • Provided by the NASA Astrophysics Data System

1984ApJ...280..825B

electron neutrinos have the shortest mean free path, their photosphere will be somewhat farther out with a lower temperature than that of the other types. In equation (57) r_{*p} is the radius of the photosphere normalized to the core radius. (In a homologous collapse, r_* is a comoving radius.) The initial value of r_{*p} is zero; it increases monotonically as the temperature rises in the interior. In a purely leptonic fireball, when interactions with nucleons can be neglected, the photosphere of the neutrinos resides at the point where $T \approx 5$ MeV. If the temperature is less, the production rate of neutrino pairs is too small to fill the allowed phase space before they can propagate away, and the interaction rate for the e^+e^- pairs present to slow down the escape by scattering reactions is also too small. The scattering rate has a steep temperature dependence for these leptonic reactions ($\sim T^5$). Above $T \sim 5$ MeV, interactions are rapid relative to the transport time and equilibration occurs. Absorption rates due to Urca reactions ($\sim T^5/s_{\rm er}$) can dominate over leptonic processes, which complicates ν_e transport.

A crude estimate for the energy loss over a dynamical time scale in this fireball phase is[1]

$$L\tau_{\rm ff} \sim 10^{56}(T/5\ {\rm MeV})^4(M_{\rm O}/100\ M_\odot)^{2/3}\rho_{c10}{}^{-7/6}\ {\rm ergs}\ . \quad (58a)$$

This compares with an entire rest mass energy $1.8 \times 10^{56} M_{\rm O}/100\ M_\odot$ ergs. We conclude that a large percentage of the gravitational binding energy may be liberated as a neutrino pulse in the last tens of milliseconds of the VMO's life before a trapped surface forms and the rest of the core accretes onto the inner black hole. The neutrino transport is clearly complicated by general relativistic effects, which tend to focus neutrino radiation upon the hole by light cone distortions and redshift the energy of the neutrinos as they leave the star.

The dynamical effects of the emitted neutrinos due to energy or momentum deposition could be significant. That the outer core material is approximately in free fall and is dominated by photons and pairs makes ejection by such mechanisms unlikely however. For the neutrino energy deposition scenario originally proposed by Colgate and White (1966) for Type II supernovae to work in these cores would require a rapid pressure increase near the core boundary followed by shock generation. The shock could be created in tightly bound regions and propagate to loosely bound ones which might then be blown off. We ignore this aspect of the scenario in the following estimate of the impact of $\nu e^\pm$ scattering on the regions outside of the photosphere. For the pressure increase, Δp, to turn free infall, characterized by the ram pressure ρv^2, into unbound outflow, the ratio $\Delta p/\rho v^2$ must exceed ~ 2. The rapid pressure gain is related to the entropy gain due to heating by $\Delta p \approx n_B T(\Delta s)_{\nu e}/3$. The rate of entropy increase at radius r_* due to electron and positron scattering of e, μ and τ neutrinos and antineutrinos radiated from the photosphere is approximately

$$(\dot{s})_{\nu e} \approx 10^3\left(\frac{T_p}{5\ {\rm MeV}}\right)^5\left(\frac{r_{*p}}{r_*}\right)^2\left(\frac{s_{\rm er}}{10}\right)\ {\rm s}^{-1}. \quad (59)$$

A relaxation approximation to νe scattering has been used to arrive at this expression, which can overestimate heating effects by up to a factor of 2, and $\nu\bar{\nu}$ reactions have been ignored. The neutrinos are assumed to have a distribution function which is blackbody at the photosphere, and is modified only by geometrical dimunition beyond. Cooling by pair emission, equation (52), will usually be smaller than this heating. To estimate the entropy gain, we take $(\Delta s)_{\nu e} \sim \dot{s}_{\nu e}\tau_{\rm ff}$, where the free-fall time scale at radius r_* and mass fraction m_* is

$$\tau_{\rm ff} \approx 0.1 r_*{}^{3/2} m_*{}^{-1/2}\rho_{c10}{}^{-1/2}\ {\rm s}\ .$$

If we assume the matter is freely infalling, which is reasonable after all the phase transitions and earlier neutrino losses, then

$$\frac{\Delta p}{\rho v^2} \approx \frac{T(\Delta s)_{\nu e}}{3m_N v_{\rm ff}{}^2(r_*)}$$
$$\sim 2\left(\frac{s_{\rm er}}{10}\right)\left(\frac{T_p}{5\ {\rm MeV}}\right)^6\frac{r_{*p}{}^{5/2}}{m_*{}^{3/2}}\left(\frac{r_*}{r_{*p}}\right)^{1/2}\left(\frac{T}{T_p}\right)\rho_{c10}{}^{-2/3}M_{\rm O2}{}^{-2/3}\ .$$

Here, $M_{\rm O2}$ is the core mass in 100 $M_\odot$ units. The maximum possible pressure increase would result if the medium were heated to T_p, for at higher temperatures the region would be thick with a new photosphere established farther out in the star. This yields

$$\frac{(\Delta p)_{\rm max}}{\rho v^2} \sim 1\left(\frac{s_{{\rm er},p}}{10}\right)\left(\frac{T_p}{5\ {\rm MeV}}\right)\frac{r_*}{m_*}\frac{\rho_p}{\rho}\rho_{c10}{}^{-2/3}M_{\rm O2}{}^{-2/3}\ .$$

The density and extremely relativistic entropy evaluated at the photosphere are labeled by p. For typical parameters, both ratios are sufficiently far below 2 that the pressure increase should not result in expulsion unless hydrodynamical transport of the energy via shocks created near the photosphere is possible; this seems unlikely. However, the pressure ratio is close enough to unity in some circumstances to warrant further study.

Since extremely relativistic particles dominate over nuclei in the outer regions, momentum deposition would also occur primarily via νe scattering. If so, the momentum change is related to the pressure change by $\Delta\rho v \approx (3/2)\Delta p$, so $\Delta(\rho v)/\rho v$ is down by

$$\sim \tfrac{3}{2}v/c \sim 0.3 m_*{}^{1/2}r_*{}^{-1/2}\rho_{c10}{}^{1/6}M_{\rm O2}{}^{1/3}$$

from the estimates of $\Delta p/\rho v^2$, making a momentum deposition supernova highly unlikely.

The collapse of rotating VMOs to black holes may provide a significant source of gravitational radiation. The luminosity can be estimated from the quadrupole formula

$$L_{\rm GW} \sim L_{\rm max}\left(\frac{GM}{Rc^2}\right)^5\left(\frac{Q}{MR^2}\right)^2,$$

where $L_{\rm max} = (2G)^{-1}c^5 \sim 10^{59}$ ergs s^{-1} is the maximum possible luminosity, the relativity parameter is $GM/Rc^2 = 0.2 M_{\rm O2}{}^{2/3}\rho_{c13}{}^{1/3}$, which is nearly unity when a trapped surface forms at ρ_{cb}, and the quadrupole ratio is

$$Q/MR^2 \sim \omega^2 R^3/GM \sim (Jc/GM^2)^2(GM/Rc^2)$$

so long as this is small. The fractional energy release over a free-fall time is then

$$\epsilon(R) \sim L_{\rm GW}\tau_{\rm ff}(Mc^2)^{-1} \sim (Jc/GM^2)^4(GM/Rc^2)^{11/2}\ .$$

One expects rotational effects to stop (or at least slow) the

[1] See note added in proof.

© American Astronomical Society • Provided by the NASA Astrophysics Data System

1984ApJ...280..825B

collapse before a trapped surface forms provided $J > GM^2/c$. This will happen at $R \sim J^2/GM^3$, when the quadrupole ratio becomes of order unity. Thereafter collapse can only proceed on the time scale with which angular momentum is lost. If the loss is entirely due to gravitational wave emission, we have $\epsilon(R) \sim GM/Rc^2$; thus ϵ can rise to a large value before a black hole forms. In the extreme case, the VMO may fission into a binary system, in which case the final burst will be generated when the components coalesce at $R \approx 6GM/c^2$; this corresponds to an efficiency parameter $\epsilon \approx 0.04$ (Clark and Eardley 1977). This contrasts with a peak efficiency $(Jc/GM^2)^4$ for collapses with $J < GM^2/c$, which occur on a free-fall time scale. However, if VMOs have an initial angular momentum characteristic of O stars, then $Jc/GM^2 \sim 200\ M_\odot/M_O$. Thus, if little angular momentum is lost during evolution, collapsing VMOs could be quite efficient generators of gravitational radiation.

The neutrino and gravitational wave pulses are the only signatures of core collapse, unless rotation can result in matter ejection either in the nuclear burning phase or later in the hole formation event itself. If metals are ejected for $M_O > M_{O_c}$, then a strong constraint can be placed upon the density of pregalactic black holes (CBA).

h) Explosion and Burn Fractions

If $M_O < M_{O_c}$, the imploding core reverses itself before significant alpha-quenching occurs. In Figure 6, V_e's for various initial entropies below the critical one are plotted. As an example, let us follow the $s_i = 12$ case: turnaround is predicted at $\rho_c \sim 7 \times 10^6$ g cm^{-3}, when about 60% of the core has burned. If we assume no further burning occurs, the effective potential can be calculated for a sequence of outflowing polytropes with the burn fractions frozen in at the turnaround value. For the outgoing sequences, V_e is steeply falling as the central density drops: the core is predicted to continue exploding, driven by the nuclear energy liberated upon infall. If the central regions have undergone some alpha-quenching as in the $s_i = 12$ case, then, as the core expands, α-particles are restructured into iron peak nuclei which liberates further nuclear potential energy to aid in the lowering of V_e. Therefore, once global outward flow begins for masses just smaller than M_{O_c}, it will continue: the mass boundary is sharply defined. Similar effective potentials allow us to predict explosion for $s_i > 8$.

The $s_i \approx 8$ adiabat just grazes the pair instability boundary. The departures from equilibrium are slight as is evidenced by the $s_i = 8$ effective potential in Figure 6. A small amount of oxygen burning is enough to turn the core around. So little oxygen is consumed that the outgoing effective potential can turn positive, which would allow for relaxation oscillations of the sort seen by Barkat, Rakavy, and Sack (1967). To treat such slight departures from hydrostatic equilibrium, detailed stellar models are required. Our $n = 3$ polytropes can only give a suggestion of the complex behavior expected near the lower VMO boundary, $M_{Om} \approx 30\ M_\odot$.

We approximate the fractions of oxygen and silicon burned by their values when the effective potential reaches zero at maximum contraction. These are plotted in Figure 3 of Bond, Arnett, and Carr (1982). The oxygen-burning fraction for VMOs is crudely fitted by

$$f_B(>\mathrm{O}) = f_O\, M_O/100\ M_\odot)^b\ ;\quad f_O \sim 0.7,\ b \sim 1.8\ . \tag{60}$$

Our results agree reasonably well with those of Barkat, Rakavy, and Sack (1967) and Fraley (1968), and with the 58 $M_\odot$ result of Arnett (1973). In the latter case, the silicon and sulfur burning products are less abundant than we would predict. As we have already noted, this is due to the structural changes which occur in the center due to oxygen burning. At the high M_O end, our results are almost a factor of 2 higher than the detailed nucleosynthetic and evolutionary calculations of Arnett (1973) and Woosley and Weaver (1982); this is compensated by our higher central densities as far as the question of global evolution is concerned.

The explosive energy generated by burning oxygen into silicon is the difference between the initial and final nuclear potential energies,

$$(\Delta V)_n = 0.9 \times 10^{53} f_B\, M_O/100\ M_\odot \text{ ergs}\ . \tag{61}$$

To get the asymptotic kinetic energy of the explosion, the binding energy of the core at the onset of instability must be subtracted from this. Since virial equilibrium holds at that point, $U_{\gamma 0} + 2U_{g0} + \Omega_{G0} = 0$. The binding energy (not including the nuclear potential) is then $U_{\gamma 0} + U_{g0} + \Omega_{G0} = -U_{g0}$. If we assume s_γ is approximately spatially independent initially, which is not unreasonable, then

$$U_{g0} = 0.5(\sigma_0 + 1)^{-1}(U_{\gamma 0} + 2U_{g0}) = -0.5\Omega_{G0}/(\sigma_0 + 1)\ ,$$

where $\sigma_0 = s_\gamma/4Y_T$ is approximately related to the oxygen core mass through equation (39). Since the gravitational potential of the core is

$$\Omega_{G0} \approx -1.3 \times 10^{53}(M_O/100\,M_\odot)^{5/3}(\rho_{c0}/10^5\ \mathrm{g\ cm^{-3}})^{1/3}\ \text{ergs}\ , \tag{62}$$

we obtain the following approximate expression for the net explosive energy:

$$\begin{aligned} K_f &= (\Delta V)_n - U_{g0} \\ &\approx 6.3 \times 10^{52}[(M_O/100\,M_\odot)^{2.8} - (M_O/100\,M_\odot)^{5/3} \\ &\quad \times (1 + \sigma_0)^{-1}]\ \text{ergs}\ . \end{aligned} \tag{63}$$

Over the explosion mass range 30–100 $M_\odot$, σ_0 varies from 1.7 up to 3.5, and ρ_{c0} from 3×10^5 down to 0.4×10^5 g cm^{-3}. Equation (63) requires $M_O > 40\ M_\odot$ in order to avoid negative values, but is useful as a first order estimate in the higher mass range. For Arnett's (1973) 58 $M_\odot$ oxygen core, we predict $K_f = 6 \times 10^{51}$ ergs; he gets 4.5×10^{51} ergs. For his 93 $M_\odot$ core, our $K_f = 3.8 \times 10^{52}$ ergs agrees with the value he got. Woosley and Weaver (1982) have followed an explosion of a 200 $M_\odot$ Population III star whose oxygen core mass is $\sim 10^2\ M_\odot$, and find $K_f = 2.6 \times 10^{52}$ ergs. We would predict our maximum possible energy output, $K_f = 4.8 \times 10^{52}$ ergs for this explosion. We are off because our burn fraction is greater than their value.

IV. DISCUSSION

The simple models of the various evolutionary stages given here, in conjunction with the detailed numerical calculations by Arnett (1973) and more recently by Woosley and Weaver (1982), Ober, El Eid, and Fricke (1982, 1983), and El Eid, Fricke, and Ober (1983), present a reasonably complete picture of nonrotating VMO evolution. The structure of VMOs can be predicted via the point source model of § II*c*. To do so requires the CNO abundance, which is

© American Astronomical Society • Provided by the NASA Astrophysics Data System

1984ApJ...280..825B

fixed for Population I and II and generated for Population III. The estimate $X_{CN} \sim 10^{-9}$ of § II*b* for metal-free stars with helium can be refined by a simple integration of the ordinary differential equation (B6) along with equation (B2). For pure hydrogen stars, the *pp* reactions must be added to generate the helium so it can in turn produce the CNO catalyst by the 3α reaction. Since $X_{CN} \sim X_\alpha^{0.8}$ in equation (14), lowering X_α from the given 0.25 of primordial nucleosynthesis to the generated value of a pure hydrogen star will lower X_{CN}, but not by much more than an order of magnitude. Pure hydrogen stars are, accordingly, only slightly hotter and smaller than pure hydrogen-helium stars, and both are substantially hotter and smaller than their Population I and II counterparts of the same mass. They are all equally bright.

A critical mass loss rate has been identified (equation [25]) above which the star remains completely convective and below which the convective core shrinks at a rate which ensures constant luminosity (equation [20]), leaving a helium core of mass $M_\alpha = M_i/(2 - X_{\alpha i})$. The helium loss in winds can then be analytically determined (equations [24]). In CBA and Bond, Carr, and Arnett (1983), we consider the conditions under which all of the primordial helium could be generated by an early population of VMOs. A catastrophic mass loss mechanism, driven by a super-Eddington luminosity generated in a hydrogen-burning shell, was identified. Exploration of the mass range over which this phenomenon occurs and the sensitivity of the outcome to the stellar population and the choice of the time-dependent convection criterion remains to be done. Will we find, for example, that a large fraction of heavy elements, especially nitrogen, will be lost along with the envelope in Population III VMOs (Woosley and Weaver 1982)? Envelope dynamics and the light curve, both of which will be sensitive to prior mass loss, need to be computed. The old issue of how pulsations influence mass loss, both in the hydrogen-burning phase and in the helium core phase if the envelope is largely stripped off, is still unresolved.

The fate of nonrotating VMOs is reasonably well established. We obtain $M_{Oc} \sim 100\ M_\odot$ within about a $10\ M_\odot$ uncertainty. Ober, El Eid, and Fricke (1983) find that their $90\ M_\odot$ O core explodes (their stellar mass at this point is $112\ M_\odot$ after mass loss), but the next one in their sequence, $\sim 110\ M_\odot$, does not. Woosley and Weaver (1982) have a $90\ M_\odot$ core which explodes, and a $105\ M_\odot$ core which just explodes. Identification of M_O in the latter case is difficult, since helium burning during the dynamical phase generated some extra carbon above what would normally be identified with the O core. Arnett's (1973) $M_O = 93\ M_\odot$ ($M_\alpha = 100\ M_\odot$) core explodes. We emphasize that our semianalytic result, first reported in Bond, Arnett, and Carr (1982), was obtained before we knew of the Ober *et al.* and Woosley and Weaver results.

Rotation drives M_{Oc} up. Unfortunately, we do not know how much angular momentum loss to expect. Typical specific angular momenta for main-sequence O stars result in triaxial instability prior to black hole formation, and could lead to complications in the simple binary collapse/explode picture of nonrotating evolution in the nuclear phase. O stars do apparently lose a substantial amount of angular momentum in their main-sequence phase, if the distribution of pulsar rotation periods can be used as a guide. Slow rotation leads to a low gravitational wave emission, but the efficiency could be large with a reasonable set of VMO core parameters. Waves from VMOs collapsing early in the universe would have redshifted to yield a small energy density now. However, by analogy with O stars, VMOs and hence their holes might often form in close binaries which could generate a large gravitational wave signal due to coalescences long after formation (Bond and Carr 1983). The enormous neutrino pulse expected at black hole birth would be currently observable in Davis's detector only for collapses within our own Galaxy.

Cosmological consequences of VMOs rely upon their black hole formation, their helium and perhaps nitrogen emission, and the large oxygen and calcium group abundances relative to iron generated by exploding VMOs. In addition, their luminous output during their nuclear and accreting hole phases, and the kinetic energy liberation via the pair supernova or super-Eddington phenomenon, can have a large impact upon the pregalactic environment (CBA). VMOs in dense star clusters could generate black holes to power active galactic nuclei. Accretion energy would presumably dominate the earlier nuclear output by a large margin.

There is some evidence that VMOs exist in less exotic sites than these, however. For example, η Car could be a VMO. It underwent an outburst in the optical in 1845. Infrared emission, due to dust reradiation in its mass loss atmosphere, now accounts for 95% of its total luminosity, which is nearly that at outburst and corresponds to the Eddington luminosity of a $220\ M_\odot$ star if its distance is 2.8 kpc (Walborn 1973; Sutton, Becklin, and Neugebauer 1974). Andriesse, Donn, and Viotti (1978) infer the enormous mass loss rate of $0.08\ M_\odot\ yr^{-1}$ since 1845. Davidson, Walborn, and Gull (1982) find that it is nitrogen-rich, suggestive of CNO processing: η Car is unlikely to be a protostar. Zwicky classified η Car as a Type V supernova. The only other example of Type V is SN 1961 in NGC 1058. Branch and Greenstein (1971) find that the ejected material is helium rich with metal abundances consistent with solar. The presupernova star was estimated to have a luminosity which would be Eddington for a $500\ M_\odot$ object (Chevalier 1981), at least from 1937 until 1961. It is classed as a slow supernova, with line widths only $\sim 2000\ km\ s^{-1}$. The super-Eddington envelope ejection of § II*e* would give the observed abundance characteristics. More study is required to determine whether the velocity and light curve characteristics can be reproduced.

Pair supernovae could be much brighter than ordinary supernovae if they retain most of their envelope, though if they are substantially stripped, as Wolf-Rayet stars apparently are, they may not be very luminous optically (Woosley and Weaver 1982). We may look forward to rare events such as pair and super-Eddington supernovae showing up in supernova searches. The influence of the $\sim 10^{52}$ ergs of shock energy on the interstellar medium will presumably mimic an explosion of ~10 normal supernovae whose shocks have summed together. The Heiles (1979) supershells have $\sim 10^{53}$ ergs; it is tempting to suggest that a few VMO explosions could aid in getting these enormous energies.

Hoyle, Solomon, and Woolf (1973) argue that the wind of a VMO will layer itself like an electron scattering atmosphere, falling off in density as radius squared. At a mass loss rate $\sim 3 \times 10^{-5}\ yr^{-1}$ all ionizing UV photons could be soaked up; the mass loss atmosphere would thus contain the entire H II region. At even higher rates, $\sim 6 \times 10^{-4}\ M_\odot\ yr^{-1}$, grain condensation in the outer

© American Astronomical Society • Provided by the NASA Astrophysics Data System

1984ApJ...280..825B

part of the atmosphere will result in a compact IR object similar to η Car. In addition, VMOs may have difficulty breaking out of their protostellar cocoons in their short nuclear lifetimes. However, the most luminous galactic IR sources are apparently not in the VMO range (Wynn-Williams 1982).

The central source, R136a, of the giant H II region 30 Doradus in the LMC is a candidate for a VMO of $\sim 2000\ M_\odot$ (Feitzinger *et al.* 1980; Cassinelli, Mathis, and Savage 1981; Meaburn *et al.* 1982). The properties of a Population I VMO of this mass are listed in Table 1. On the other hand, the central region could represent a young globular cluster core in which many O stars and Wolf-Rayet stars reside (Melnick 1983). Massey and Hutchings (1983) find that many other giant H II regions have R136a type objects, suggesting the phenomenon may be widespread. Whatever the resolution to the R136a puzzle is, it will be of interest to VMO research, for Larson (1982) has found that the maximum star mass in a star-forming region rises with the cloud mass. It has already been established that there are some $\sim 100\ M_\odot$ stars in the LMC.

We thank Willy Fowler, Lee Lindblom, Wolfgang Ober, Bob Wagoner, and Stan Woosley for useful discussions. In particular, Stan Woosley often emphasized the many ways rotation could transform simplicity into complexity. This research was supported by grants NSF AST-80-22876 at Chicago, NSF AST 79-23243 at Berkeley, and NSF PHY 81-19387 at Stanford, and by the SERC at Cambridge.

APPENDIX A

CENTRAL TEMPERATURE DURING HYDROGEN BURNING

Once the CNO abundance has been generated, the specific nuclear emissivity due to the CNO cycle, $\dot{q}_{\rm CN}$, is determined by the rate-limiting step $^{14}{\rm N}(p,\gamma)^{15}{\rm O}$ and is given by

$$\dot{q}_{\rm CN} = \rho X_p X_{\rm N} E(T)\,,$$
$$E(T) = Q(1-v) f \langle \sigma v \rangle m_N{}^{-1}/14$$
$$\approx 10^{-2} T^{-2/3} \exp\left[67.3(1 - T^{-1/3})\right] \text{ ergs g}^{-1}\text{ s}^{-1}\,.$$

$E(T)$ is related to the reaction rate $\langle \sigma v \rangle$, the energy release in the CNO cycle, $Q = 26.73$ MeV, the fraction of energy carried off by neutrinos, $v = 0.06$, and the screening factor f, which is unity in this regime of extremely weak screening. If CNO nuclei have their equilibrium abundances, then the ^{14}N abundance is approximately given by $X_{\rm N} = X_{\rm CNO}$. It is instructive to make a power law fit to $E(T)$ in the neighborhood of the central temperature T_c:

$$\dot{q}_{\rm CN} \approx 0.048\, Y_T{}^{-1} X_p X_{\rm CN} E(T_c) T_c{}^3 \sigma^{-1} (T/T_c)^{\nu}\,;$$
$$\nu_p(T_c) \equiv \left(\frac{\partial \ln \dot{q}_{\rm CN}}{\partial \ln T}\right)_{s_\gamma} = 22.42 T_c{}^{-1/3} + \frac{7}{3}$$

ranges from 18 for Population I VMOs down to 12 for Population III VMOs. This dependence is steep enough to ensure that energy transport from the central regions must take place convectively. The mean energy generation rate is related to its central value by

$$\langle \dot{q} \rangle / \dot{q}_c = \int (s_\gamma / s_{\gamma c})^{(\nu_p/3 - 1)} (\rho/\rho_c)^{\nu_p/3} dm/M\,.$$

Since most of the generation occurs in the central regions, we can follow Fowler and Hoyle (1964) and use the result for polytropes of index n that

$$\rho/\rho_c \approx \exp\left(-n\xi^2/6\right) \tag{A1}$$

near the center. For an $n = 3$ polytrope, $\xi = 6.9 r/R$ and $dm/M = (\rho/\rho_c)\xi^2 d\xi/2.01824$. As long as $\nu_p{}^2/(72 s_{\gamma c})$ is small, and the integrand is highly peaked in the center, so we can extend the range of integration from 0 to ∞, we obtain

$$\langle \dot{q} \rangle / \dot{q}_c = \pi^{1/2} [4(2.01824)]^{-1} [1 + (\nu_p - 3)/6(1+e)]^{-3/2}\,,$$
$$e = (2 s_{\gamma c}/Y_N + 1)^{-1}\,. \tag{A2}$$

The correction term e arises from the variation in s_γ expressed by equation (16). It is small for large-mass stars, and results in only a slight deviation from the expression given by Fowler and Hoyle (1964) for $n = 3$ polytropes. If we now use equation (9) for $\langle \dot{q} \rangle = L/M$, we obtain an expression for $E(T_c) T_c{}^3$ in terms of s_γ, which reduces to the transcendental equation:

$$T_c = 2.67 \text{ keV } (1 - 0.021 \ln A - 0.021 \ln X_{\rm Nc}{}^{-1} + 0.053 \ln T_c)^{-3}\,;$$
$$A = s_{\gamma c} [1 + (\nu_p - 3)(1+e)/6]^{3/2} [Y_{pc}\, Y_{ec} (1 + \sigma^{-1})]^{-1}\,. \tag{A3}$$

© American Astronomical Society • Provided by the NASA Astrophysics Data System

1984ApJ...280..825B

An approximate expression for T follows by exploiting the smallness of the ln A term, and using $1 + \epsilon \ln A = A^{\epsilon}$ for small ϵ:

$$T_c = (2.67)^p A^{3pk}(1 + 0.021 \ln X_N)^{-3p} \text{ keV},$$
$$k = 0.021/(1 + 0.021 \ln X_N),$$
$$p = (1 + 0.021 \ln X_N)/(1.159 + 0.021 \ln X_N). \quad \text{(A4)}$$

A simple expression follows if the ln X_N term is also small:

$$T_c = 2.33(A/X_N)^{1/18.4} \text{ keV}, \quad \text{(A5a)}$$

which is quite adequate for Population I and II abundances (low by a few percent), but gives a temperature too low by 25% for the Population III value, $X_N = 10^{-9}$. However, if we treat ln $(X_N/10^{-9})$ as a small term, we obtain the Population III temperature relation

$$T_c = 8.2A^{0.0871}(X_N/10^{-9})^{-(0.0698+0.0025 \ln A)} \text{ keV}. \quad \text{(A5b)}$$

We have inserted typical zero-age main sequence values for the abundances to obtain equations (11a) and (11b). The rise in temperature as Y_p and Y_e drop in the center is predicted by the A dependence.

APPENDIX B

THE CNO ABUNDANCE IN POPULATION III STARS

In order to calculate the CNO abundance generated in Population III stars, we need to evaluate the energy equation,

$$\frac{d}{dt}\frac{E}{M} + \frac{L}{M} = \langle \dot{q}_{3\alpha} + \dot{q}_{CN} \rangle \quad \text{(B1)}$$

which gives the central temperature evolution, in conjunction with

$$\frac{d}{dt}\langle X_{CN} \rangle = \frac{\langle \dot{q}_{3\alpha} \rangle m_N}{Q_{3\alpha}}, \quad \text{(B2)}$$

which gives the production rate of ^{12}C nuclei; we can assume ^{12}C is immediately processed into ^{14}N by the CNO reactions. Here, $Q_{3\alpha} = 606$ keV is the energy liberated per baryon in He burning, and

$$\dot{q}_{3\alpha} = 5 \times 10^{11} \frac{X_\alpha{}^3}{Y_T{}^2} \frac{T^3}{\sigma^2} \exp\left(-\frac{380.2}{T}\right) \text{ ergs g}^{-1} \text{ s}^{-1} \quad \text{(B3a)}$$

$$= 2.2 \times 10^7 \frac{X_\alpha{}^3}{Y_T{}^2 \sigma^2} \left(\frac{T}{20 \text{ keV}}\right)^{22} \text{ ergs g}^{-1} \text{ s}^{-1}. \quad \text{(B3b)}$$

The power of T is more generally

$$\nu_\alpha \equiv \left(\frac{\partial \ln \dot{q}_{3\alpha}}{\partial \ln T}\right)_{s_\gamma} = \frac{380.2 \text{ keV}}{T} + 3. \quad \text{(B3c)}$$

The average of the 3α energy generation can be related to its central value in the same way as for CNO burning (equation [A2]). The energy is evaluated by assuming that the virial theorem holds:

$$E/M = -3Y_T \langle T \rangle/(2m_N) = -3Y_T F_T T_c/(2m_N). \quad \text{(B4)}$$

The form factor for the mean temperature can be obtained by using the Gaussian approximation, equation (A1):

$$F_T = \frac{\int (\sigma/\sigma_c)^{1/3}(\rho/\rho_c)^{4/3}\xi^2 d\xi}{\int (\rho/\rho_c)\xi^2 d\xi} \approx \left(\frac{3}{4+e}\right)^{3/2} \approx 0.65. \quad \text{(B5)}$$

The correction factor $e = (8\sigma + 1)^{-1}$ is neglected in the last step.

Equations (B1) and (B2) can be combined to yield an expression for T_c in terms of the independent variable X_{CN} which is a monotonically increasing function of time:

$$\frac{3}{2}\frac{F_T}{Q_{3\alpha}}\frac{dT_c}{dX_{CN}} = \frac{1 - M\langle \dot{q}_{3\alpha} \rangle/L - M\langle \dot{q}_{CN} \rangle/L}{M\langle \dot{q}_{3\alpha} \rangle/L}. \quad \text{(B6)}$$

Since $\langle \dot{q}_{CN} \rangle \propto X_{CN}$, this equation cannot be evaluated analytically. In the initial phases of evolution, the temperature rises due to Kelvin-Helmholtz contraction. The 3α reactions only slightly modify the evolution. The curve

$$X_{CN}(T_c) = -\frac{3}{2} F_T \frac{T_c}{Q_{3\alpha}} \frac{1}{(\nu_\alpha + 1)} \ln\left(1 - \frac{M\langle \dot{q}_{3\alpha} \rangle}{L}\right) \quad \text{(B7)}$$

© American Astronomical Society • Provided by the NASA Astrophysics Data System

1984ApJ...280..825B

describes this behavior. It is an approximate solution to equation (B6) with the CNO contribution neglected. Another limiting case occurs along the line in T_c–X_{CN} space defined by thermal equilibrium, when nuclear energy generation can support the star:

$$X_{CN}^{eq}(T_c) = (1 - M\langle \dot{q}_{3\alpha}\rangle/L)(M(\langle \dot{q}_{CN}\rangle X_{CN}^{-1})/L)^{-1} . \tag{B8}$$

The right-hand side is a function of T_c only. When X_{CN} is negligible, equation (B8) reduces to the equilibrium temperature for helium burning,

$$T_{eq\alpha} \approx 9.64\left(\nu_\alpha + \frac{3}{2}\right)(\nu_\alpha - 3)\left[1 - 0.0254 \ln\left\{(\nu_\alpha - 3)^3(\nu_\alpha + 3)^{3/2}\left[\frac{Y_T^2\sigma^3}{Y_e X_\alpha^3(1+\sigma)}\right]\right\}\right]^{-1} \text{keV} . \tag{B9}$$

This expression is a relatively accurate solution to the transcendental equation for $T_{eq\alpha}$. If we use $\nu_\alpha = 22$, we have

$$T_{eq\alpha} \approx 18.3\left(\frac{Y_T^2}{X_\alpha^3 Y_e}\right)^{1/25.8}\left(\frac{\sigma^2}{1+\sigma^{-1}}\right)^{1/25.8} \text{keV} . \tag{B10}$$

For $X_\alpha = 1$, the coefficient is 18.3 keV. This is the expression used in equation (30) for the ignition temperature of helium. If $X_\alpha = 0.24$, the coefficient is 22.6 keV. This is substantially above the temperatures characteristic of equilibrium CNO burning for $X_{CN} \sim 10^{-9}$, and suggests $\langle \dot{q}_{3\alpha}\rangle \ll L/M$. When we ignore this contribution, equation (B8) reduces to the T_c–X_{CN} relations, equations (A5) and (11).

The actual evolution will follow equation (B7) initially, deviating from it as X_{CN} rises, and finally will match onto the curve given by equation (B8). Thus, an approximation to the true trajectory is to follow the contraction curve until it intersects the thermal equilibrium curve. The intersection point satisfies

$$\tilde{X}_{CN} = \frac{M}{L}\langle \dot{q}_{3\alpha}(T_{eq,p}(\tilde{X}_{CN}))\rangle \frac{3F_T}{2(\nu_\alpha + 1)}\frac{T_{eq,p}(\tilde{X}_{CN})}{Q_{3\alpha}} . \tag{B11}$$

We have used the smallness of the helium contribution to get this. Using equation (A5) for $T_{eq,p}(\tilde{X}_{CN})$, we finally obtain equation (14).

Once the star has settled upon the equilibrium T_c–X_{CN} line, there is slow evolution following equation (B2). We now expand the 3α generation rate about 15 keV since this is more characteristic of equilibrium hydrogen burning temperatures than 20 keV. After time t, the N abundance is

$$X_{CN}(t) \approx X_{CN}(0)\{1 + (t/10^4 \text{ yr})\sigma^{2.94}(1+\sigma)^{-2.47}[X_{CN}(0)/10^{-9}]^{3.24}\}^{0.31} . \tag{B12}$$

The abundance does not take very long to exceed 10^{-9}.

APPENDIX C

THE POLYTROPIC MASS CORRECTION FACTOR

We can understand the form and magnitude of the function $F_M(\sigma)$ by explicitly taking into account deviations of the photon entropy from its central value. The polytropic mass is obtained from the virial equation: $3Pv = (3/2)GM^2/R$. Two corrections enter due to deviations: one is the modification of the gravitational potential which we ignore; the other is the correction to $\bar{P}v$,

$$F_p = \frac{\int s_\gamma^{4/3}(1+\sigma^{-1})(\rho/\rho_c)^{1/3}dm/M}{s_{\gamma c}^{4/3}(1+\sigma_c^{-1})\int(\rho/\rho_c)^{1/3}dm/M} .$$

Using the approximation equation (A1) and the relation $F_M \sim F_p^{3/2}$, we obtain

$$F_M(\sigma) = \frac{(1+\sigma^{-1}[[[1+(1+8\sigma)^{-1}]\{1+[4(1+8\sigma)]^{-1}\}^{-1}]^{3/2})^{3/2}}{[1+(1+8\sigma)^{-1}]^{3/4}(1+\sigma^{-1})^{3/2}} ,$$

a remarkably accurate fit to Henrich's numerical result. A very accurate approximation to the M–σ_c relation is

$$M(\sigma_c) = 17.6 Y_T^2 \sigma_c^{1/2}(\sigma_c + \tfrac{39}{64})^{3/2} . \tag{C1}$$

Equation (15) inverts this expression for $M > 100\ M_\odot$.

REFERENCES

Andriesse, C. D., Donn, B. D., and Viotti, R. 1978, *M.N.R.A.S.*, **185**, 771.
Appenzeller, I. 1970, *Astr. Ap.*, **9**, 216.
Appenzeller, I., and Tscharnuter, W. 1974, *Astr. Ap.*, **30**, 423.
Arnett, W. D. 1972, *Ap. J.*, **176**, 681.
———. 1973, in *Explosive Nucleosynthesis*, ed. W. D. Arnett and D. N. Schramm (Austin: University of Texas Press).
———. 1977, *Ap. J. Suppl.*, **35**, 145.
Arnett, W. D., Bond, J. R., and Carr, B. J. 1982, Proc. Munich Conference on Massive Stars.
Barkat, Z., Rakavy, G., and Sack, N. 1967, *Phys. Rev. Letters*, **18**, 379.
Begelman, M. C., and Rees, M. J. 1978, *M.N.R.A.S.*, **185**, 847.
Bludman, S. 1973, *Ap. J.*, **183**, 637.
Bodansky, D., Clayton, D. D., and Fowler, W. A. 1968, *Ap. J. Suppl.*, **16**, 299.

© American Astronomical Society • Provided by the NASA Astrophysics Data System

1984ApJ...280..825B

Bodenheimer, P., and Ostriker, J. 1973, *Ap. J.*, **180**, 159.
Bond, J. R., Arnett, W. D., and Carr, B. J. 1982, in *Supernovae*, ed. M. J. Rees and R. J. Stoneham (Dordrecht: Reidel).
Bond, J. R., and Carr, B. J. 1983, *M.N.R.A.S.*, in press.
Bond, J. R., Carr, B. J., and Arnett, W. D. 1983, *Nature*, **304**, 514.
Boury, A. 1963, *Ann. d'Ap.*, **26**, 354.
Branch, D., and Greenstein, J. L. 1971, *Ap. J.*, **167**, 89.
Carr, B. J., Arnett, W. D., and Bond, J. R. 1982, in *Supernovae*, ed. M. J. Rees and R. J. Stoneham (Dordrecht: Reidel).
Carr, B. J., Bond, J. R., and Arnett, W. D. 1984, *Ap. J.*, **277**, in press (CBA).
Cassinelli, J. P., Mathis, J. S., and Savage, B. D. 1981, *Science*, **212**, 1497.
Chevalier, R. 1981, *Fund. Cosmic Phys.*, **7**, 1.
Clark, J. P. A., and Eardley, D. M. 1977, *Ap. J.*, **215**, 311.
Colgate, S. A., and White, R. H. 1966, *Ap. J.*, **143**, 626.
Cox, J. P., and Giulli, R. T. 1968, *Principles of Stellar Structure* (New York: Gordon & Breach).
Davidson, K., Walborn, N. R., and Gull, T. R. 1982, *Ap. J.* (*Letters*), **254**, L47.
Deinzer, W., and Salpeter, E. E. 1964, *Ap. J.*, **140**, 499.
Duncan, M. J., and Shapiro, S. L. 1983, *Ap. J.*, **268**, 565.
El Eid, M. F., Fricke, K. J., and Ober, W. W. 1983, *Astr. Ap.*, **119**, 54.
Feitzinger, J. V., Schlosser, W., Schmidt-Kaler, Th., and Wrinkler, C. 1980, *Astr. Ap.*, **84**, 50.
Fowler, W. A. 1966, *Ap. J.*, **144**, 180.
Fowler, W. A., Caughlin, G. R., and Zimmerman, B. A. 1975, *Ann. Rev. Astr. Ap.*, **13**, 69 (FCZ II).
Fowler, W. A., and Hoyle, F. 1964, *Ap. J. Suppl.*, **9**, 201.
Fraley, G. S. 1968, *Ap. Space Sci.*, **2**, 96.
Fricke, K. J. 1973, *Ap. J.*, **183**, 941.
———. 1974, *Ap. J.*, **189**, 535.
Hartquist, T. W., and Cameron, A. G. W. 1977, *Ap. Space Sci.*, **48**, 140.
Heiles, C. 1979, *Ap. J.*, **229**, 553.
Henrich, L. R. 1943, *Ap. J.*, **98**, 192.
Hoyle, F., Solomon, P. M., and Woolf, N. J. 1973, *Ap. J.* (*Letters*), **185**, L89.
Hutchins, J. B. 1976, *Ap. J.*, **205**, 103.
Ikeuchi, S. 1981, *Pub. Astr. Soc. Japan*, **33**, 211.
Kashlinsky, A., and Rees, M. J. 1983, preprint.
Kovetz, A., and Shaviv, G. 1971, *Ap. Space Sci.*, **14**, 378.
Larson, R. B. 1982, *M.N.R.A.S.*, **200**, 159.
Larson, R. B., and Starrfield, S. 1971, *Astr. Ap.*, **13**, 190.
Ledoux, P. 1941, *Ap. J.*, **94**, 537.
Massey, P., and Hutchings, J. B. 1983, DAO preprint.
Meaburn, J., Hebden, J. C., Morgan, B. L., and Vine, H. 1982, *M.N.R.A.S.*, **200**, 1P.
Melnick, J. 1983, *ESO Messenger*, **32**, 11.
Ober, W. W., El Eid, M. F., and Fricke, K. J. 1982, in *Supernovae*, ed. M. J. Rees and R. J. Stoneham (Dordrecht: Reidel).
———. 1983, *Astr. Ap.*, **119**, 61.
Ostriker, J. P., and Cowie, L. L. 1981, *Ap. J.* (*Letters*), **243**, L127.
Palla, F., Salpeter, E. E., and Stahler, S. W. 1983, Cornell preprint CRSR 804.
Papaloizou, J. C. B. 1973, *M.N.R.A.S.*, **162**, 169.
Rakavy, G., and Shaviv, G. 1968, *Ap. Space Sci.*, **1**, 429.
Schwarzschild, M., and Härm, R. 1958, *Ap. J.*, **128**, 348.
———. 1959, *Ap. J.*, **129**, 637.
Silk, J. 1977, *Ap. J.*, **211**, 638.
———. 1980, in *Star Formation, 10th Saas Fee Course*, ed. I. Appenzeller, J. Lequeux, and J. Silk (Geneva: Geneva Observatory), p. 133.
Stothers, R. 1972, *Ap. J.*, **175**, 431.
Stothers, R., and Simon, N. R. 1970, *Ap. J.*, **160**, 1019.
Sutton, E., Becklin, E., and Neugebauer, G. 1974, *Ap. J.* (*Letters*), **190**, L69.
Talbot, R. J. 1971, *Ap. J.*, **165**, 121.
Talbot, R. J., and Arnett, W. D. 1971, *Nature*, **229**, 150.
Tohline, J. E. 1980, *Ap. J.*, **239**, 417.
Tooper, R. F. 1964, *Ap. J.*, **140**, 434.
Wagoner, R. V. 1969, *Ann. Rev. Astr. Ap.*, **7**, 553.
Walborn, N. R. 1973, *Ap. J.*, **179**, 517.
Weaver, T. A., and Woosley, S. E. 1980, *Ann. NY Acad. Sci.*, **336**, 335.
Weaver, T. A., Zimmerman, G. B., and Woosley, S. E. 1978, *Ap. J.*, **225**, 1021.
Wheeler, J. C. 1977, *Ap. Space Sci.*, **50**, 125.
Woody, D., and Richards, P. L. 1979, *Phys. Rev. Letters*, **42**, 925.
Woosley, S. E., Arnett, W. D., and Clayton, D. D. 1973, *Ap. J. Suppl.*, **231**, 231.
Woosley, S. E., and Weaver, T. A. 1982, in *Supernovae*, ed. M. J. Rees and R. J. Stoneham (Dordrecht: Reidel).
Wynn-Williams, C. G. 1982, *Ann. Rev. Astr. Ap.*, **20**, 587.
Yoneyama, T. 1972, *Pub. Astr. Soc. Japan*, **24**, 87.
Yorke, H. W., and Krügel, E. 1977, *Astr. Ap.*, **54**, 183.
Zel'dovich, Ya. B., and Novikov, I. D. 1971, *Relativistic Astrophysics* (Chicago: University of Chicago Press).
Ziebarth, K. 1970, *Ap. J.*, **162**, 947.

Note added in proof.—Consider instead the assumption that all regions which achieve a temperature in excess of 5 MeV have the neutrinos strongly trapped. In that case, the maximum possible energy which could be radiated is the thermal energy content per baryon at $T = 5$ MeV: $(3s_{er}/4 + 3Y_T/2)$ 5 MeV. In the optimal case, this energy would be radiated before the nuclear phase transitions have lowered s_{er} much below s. Relating s_{er} to the core mass leads to the bound

$$E_\nu < 10^{55}(M_O/100\ M_\odot)^{3/2}\ \text{ergs}\ , \tag{58b}$$

which can be less than the estimate of equation (58a).

W. DAVID ARNETT: Astronomy and Astrophysics Center, University of Chicago, 5640 S. Ellis Ave., Chicago, IL 60637

J. RICHARD BOND: Physics Department, Stanford University, Stanford, CA 94305

BERNARD J. CARR: Institute of Astronomy, Madingley Road, Cambridge University, Cambridge CB3 0HA, England

© American Astronomical Society • Provided by the NASA Astrophysics Data System